Article

Cell Reports

β-aminoisobutyric Acid, L-BAIBA, Is a Muscle-Derived Osteocyte Survival Factor

Graphical Abstract

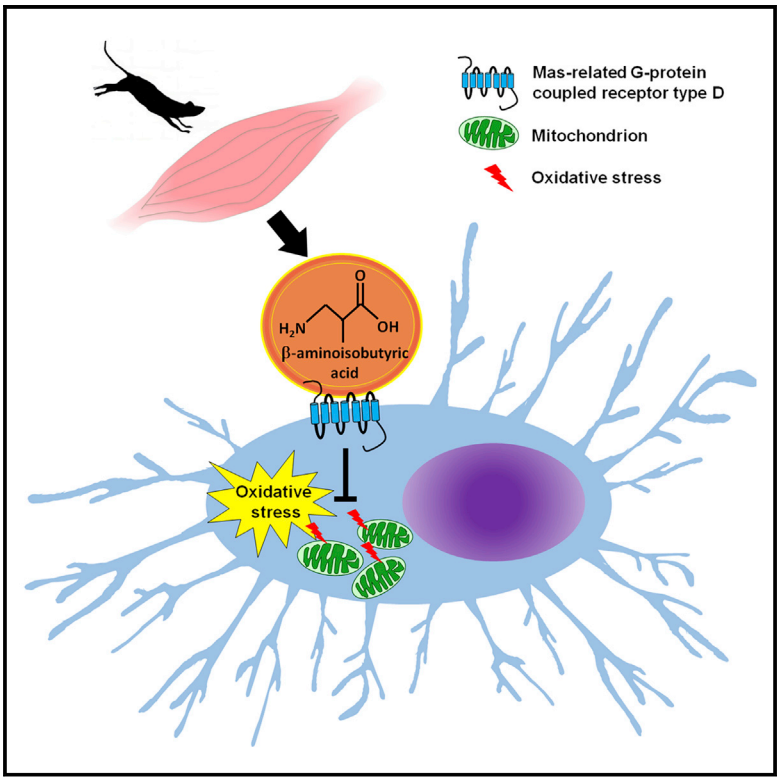

Authors

Yukiko Kitase, Julian A. Vallejo, William Gutheil, ..., Jingsong Zhou, Marco Brotto, Lynda F. Bonewald

Correspondence

kitasey@iu.edu (Y.K.), lbonewal@iu.edu (L.F.B.)

In Brief

Kitase et al. show that the muscle-derived factor L-BAIBA signals through the MRGPRD to prevent osteocyte cell death induced by reactive oxygen species, a function lost with aging.

Highlights

- The muscle metabolite L-BAIBA protects osteocytes from ROS-induced cell death
- L-BAIBA prevents mitochondrial breakdown in osteocytes
- The effects of L-BAIBA are mediated via MRGPRD that decreases with aging
- *In vivo*, L-BAIBA reduces bone and muscle loss resulting from immobilization

Kitase et al., 2018, Cell Reports *22*, 1531–1544
February 6, 2018
https://doi.org/10.1016/j.celrep.2018.01.041

CellPress

Cell Reports
Article

β-aminoisobutyric Acid, L-BAIBA, Is a Muscle-Derived Osteocyte Survival Factor

Yukiko Kitase,[1,*] Julian A. Vallejo,[2,3] William Gutheil,[4] Harika Vemula,[4] Katharina Jähn,[5] Jianxun Yi,[6] Jingsong Zhou,[6] Marco Brotto,[7] and Lynda F. Bonewald[1,8,9,*]

[1]Department of Anatomy and Cell Biology, School of Medicine, Indiana University, Indianapolis, IN 46202, USA
[2]Department of Biomedical Sciences, School of Medicine, University of Missouri-Kansas City, Kansas City, MO 64108, USA
[3]Department of Oral & Craniofacial Sciences, School of Dentistry, University of Missouri-Kansas City, Kansas City, MO 64108, USA
[4]Division of Pharmaceutical Sciences, School of Pharmacy, University of Missouri-Kansas City, Kansas City, MO 64108, USA
[5]Department of Osteology and Biomechanics, University of Medical Center Hamburg-Eppendorf, Hamburg, Germany
[6]Kansas City University of Medicine and Bioscience, Kansas City, MO 64106, USA
[7]Bone-Muscle Collaborative Science, College of Nursing & Health Innovation, University of Texas-Arlington, Arlington, TX 76019, USA
[8]Department of Orthopaedic Surgery, School of Medicine, Indiana University, Indianapolis, IN 46202, USA
[9]Lead Contact
*Correspondence: kitasey@iu.edu (Y.K.), lbonewal@iu.edu (L.F.B.)
https://doi.org/10.1016/j.celrep.2018.01.041

SUMMARY

Exercise has beneficial effects on metabolism and on tissues. The exercise-induced muscle factor β-aminoisobutyric acid (BAIBA) plays a critical role in the browning of white fat and in insulin resistance. Here we show another function for BAIBA, that of a bone-protective factor that prevents osteocyte cell death induced by reactive oxygen species (ROS). L-BAIBA was as or more protective than estrogen or N-acetyl cysteine, signaling through the Mas-Related G Protein-Coupled Receptor Type D (MRGPRD) to prevent the breakdown of mitochondria due to ROS. BAIBA supplied in drinking water prevented bone loss and loss of muscle function in the murine hindlimb unloading model, a model of osteocyte apoptosis. The protective effect of BAIBA was lost with age, not due to loss of the muscle capacity to produce BAIBA but likely to reduced *Mrgprd* expression with aging. This has implications for understanding the attenuated effect of exercise on bone with aging.

INTRODUCTION

Clearly, exercise has beneficial effects on many systems in the body, such as the neural, metabolic, and musculoskeletal systems (Blair et al., 1995), but it is not clear if these benefits delay the effects of aging or if aging blunts the effects of exercise. Sarcopenia and osteoporosis are major hallmarks of the aging musculoskeletal system, resulting in frailty, falls, fracture, and morbidity. It is predicted that 1 in 5 individuals will be over the age of 65 by 2020 (Benefield and Holtzclaw, 2014); therefore, it becomes imperative to understand these two co-morbidities in order to prevent both muscle and bone weakness.

Bone and muscle have an intimate relationship and show synchronization of tissue mass throughout life, from development to old age (Brotto and Bonewald, 2015). Exercise maintains or increases both bone and muscle mass, whereas disuse results in a reduction in mass/function of both tissues. Exercise has less of an anabolic effect on the bone with aging. Muscle and bone clearly have a mechanical interaction, with muscle loading the bone for locomotion, but recently it has been shown these tissues communicate through secreted factors. Factors have been identified as secreted by bone cells, such as osteocalcin (Karsenty and Olson, 2016), and secreted by osteocytes, such as prostaglandins (Mo et al., 2012) and WNTs (Huang et al., 2017), which have effects on muscle. Contracted muscle-derived factors, such as insulin growth factor-1 (IGF-1), fibroblast growth factor-2 (FGF-2) (Hamrick et al., 2010), interleukin-15 (IL-15) (Nielsen et al., 2007), and irisin (Colaianni et al., 2015), have osteogenic effects. In contrast, disuse-induced muscle atrophy produces myostatin that has anti-osteogenic effects by decreasing osteoblastogenesis (Qin et al., 2017) and increasing osteoclastogenesis (Dankbar et al., 2015). These findings support the concept of muscle/bone communication.

Our group has focused on the bone cell embedded in the bone matrix, the osteocyte. Osteocytes derive from a subpopulation of osteoblasts by the embedding into the newly formed bone and the formation of a global mechanosensory cellular network inside the bone matrix. This cell has come from obscurity a decade ago to being recognized as a multifunctional cell (Bonewald, 2011) that can regulate osteoclasts, the bone-resorbing cells, through RANKL expression (Nakashima et al., 2011; Xiong et al., 2015), and osteoblasts, the bone-forming cells, through sclerostin production (van Bezooijen et al., 2004) and WNT1 (Joeng et al., 2017). Osteocytes as endocrine cells have been shown to target the kidney through fibroblast growth factor-23 (Feng et al., 2003) by binding the FGF receptor/Klotho complex (Urakawa et al., 2006) to regulate phosphate excretion by the kidney. Unlike osteoblasts and osteoclasts, which are viable from days to a few weeks, osteocytes are viable for decades in the bone matrix. Osteocyte death can signal resorption and remodeling of bone; therefore, maintenance of osteocyte viability requires tight control. A number of factors have been shown to

cause osteocyte cell death, such as IL-1, tumor necrosis factor alpha (TNF-α), glucocorticoids, reactive oxygen species (ROS), and others, and to prevent the effects of these factors, a number of protective factors have been shown to prevent osteocyte cell death, such as estrogen, parathyroid hormone, N-acetyl cysteine (NAC), and others (Jilka et al., 2013). However, these protective factors are not regulated by exercise, so we postulated that muscle secretes osteocyte-protective factors in response to contraction. We had previously shown that muscle is a source of osteocyte-protective factors, and we showed that contracted muscle secretes factors that protect osteocytes against glucocorticoid-induced cell death (Jähn et al., 2012). Here we identify β-aminoisobutyric acid (BAIBA) as a major osteocyte-protective factor.

In 2014, BAIBA was described as a small (103.6-Da) molecule produced by skeletal muscle during exercise (Roberts et al., 2014), and it was shown to signal the beneficial effect of exercise from skeletal muscle to other tissues and organs in an endocrine manner. BAIBA increases energy expenditure by activating the β-oxidation pathway of hepatic fatty acid, triggers the browning of white adipose tissue, is inversely correlated with cardiometabolic risks factors (Roberts et al., 2014), and improves insulin resistance and inflammation in skeletal muscle in an autocrine/paracrine manner (Jung et al., 2015). More recently, the molecule has been shown to reduce hepatic endoplasmic reticulum (ER) stress and glucose/lipid metabolic disturbance in type 2 diabetes (Shi et al., 2016) and to ameliorate renal fibrosis, in a mouse model of obstructed kidney, via the inhibition of renal fibroblast activation and fibrosis (Wang et al., 2017).

Here we describe another function for BAIBA as a muscle-secreted factor that protects osteocytes against ROS and can prevent both bone and muscle loss *in vivo*. We identified and describe the mechanism used by this factor to protect osteocytes, via signaling through the Mas-related G protein-coupled receptor type D (MRGPRD), to prevent mitochondrial breakdown in osteocytes. We also describe how this function of BAIBA is lost with aging, not through the muscle capacity to produce BAIBA with contraction but through the downregulation of this receptor in osteocytes. These findings have implications for correcting reduced skeletal response to exercise with aging and for muscle-bone interactions during aging.

RESULTS

Muscle Secretes Osteocyte-Protective Factors

Previously we hypothesized that muscle and bone communicate through soluble factors (Bonewald et al., 2013), and then we showed that osteocytes produce factors that support myogenesis and muscle function (Mo et al., 2012) and that muscle secretes osteocyte-protective factors (Jähn et al., 2012). As C2C12 myotube conditioned media (CM) mimicked the effects of extensor digitorum longus (EDL) and soleus (SOL) CM (Figure 6 of Jähn et al., 2012) with regard to osteocyte-protective capability, a series of fractionation experiments were performed. The bioactivity was less than 10 kDa (even less than 3 kDa), resistant to trypsin and boiling, and partially degraded by UV light over time (Figures S1A and S1B). As we have demonstrated previously that PGE_2 is a potent anti-apoptotic agent and is highly expressed by osteocytes in response to fluid flow shear stress (Kitase et al., 2010), we measured PGE_2 levels in muscle CM. CM from C2C12 myoblasts or myotubes and both EDL and soleus with and without contraction presented with low levels of PGE_2, insufficient to have an effect on osteocytes (MLO-Y4 cells subjected to 2 dynes/cm^3 fluid flow shear stress produced 18,353 ± 1,969, C2C12 myotube-CM 168 ± 10, and C2C12 myoblast-CM 63 ± 4 PGE_2 pg/10^6 cells; experiments were repeated 3 times with similar results).

As ROS are elevated with aging, we next determined if muscle-secreted factors could protect against ROS-induced osteocyte cell death. Both static and contracted EDL and soleus CM were protective (Figure S2). We screened a number of small molecular weight molecules secreted by muscle, including BAIBA, for their protective capacity using the osteocyte cell line MLO-Y4, and BAIBA was the most potent (Figure 1A). The L-isoform was shown to be the more active form compared to the D-isoform (Figure 1A), and L-BAIBA was as or more potent than the well-known anti-apoptotic factors β-estradiol and NAC (Figure 1B). ROS was shown to be reduced by both L-BAIBA and the positive control NAC (Figure 1C). Catalase and Gpx4, known to protect against ROS, were increased in response to L-BAIBA, similar to NAC (Figure 1D). We have also examined the protective effect of BAIBA on osteoblasts as precursors of osteocytes using an osteoblast cell model, MC3T3-E1, and we found that it also prevented them from cell death induced by hydrogen peroxide (Figure S3).

L-BAIBA Protects against Bone and Muscle Loss due to Disuse

To understand the *in vivo* relevance of the cellular effects determined *in vitro*, experiments were performed using the established murine hindlimb unloading model in which the detrimental effects of unloading on bone mass through apoptotic osteocytes is well described (Basso and Heersche, 2006). Blocking osteocyte apoptosis using an apoptosis inhibitor has been shown to prevent bone loss induced by hindlimb unloading (Cabahug-Zuckerman et al., 2016). As BAIBA production is increased with exercise (Roberts et al., 2014), the hindlimb unloading assay, a model for disuse or lack of exercise, was performed to determine if BAIBA could prevent bone loss. Hindlimb unloading was performed for 2 weeks on paired 5-month-old males or 3-month-old females with or without 100 mg/kg/day L-BAIBA added to drinking water (3-month-old females were chosen because of almost complete loss of trabecular bone by 5 months of age).

At baseline, both groups showed no statistical differences in trabecular parameters in the tibial metaphysis. Also at baseline, both groups showed no statistical differences in Ellipsoid factor (EF) values categorized in each structure showing plate-type-dominated structures (control, 50.3% ± 6.8%; L-BAIBA, 45.1% ± 7.6% in male; control, 31.2% ± 11.4%; L-BAIBA, 38.912.42% in female) and intermediate structures (control, 49.5% ± 6.8%; L-BAIBA, 54.4% ± 7.8% in male; control, 64.0% ± 11.7%; L-BAIBA, 59.8% ± 15.4% in female). *In vivo* micro computed tomography (μCT) analysis at two time points showed that hindlimb-unloaded mice given L-BAIBA have

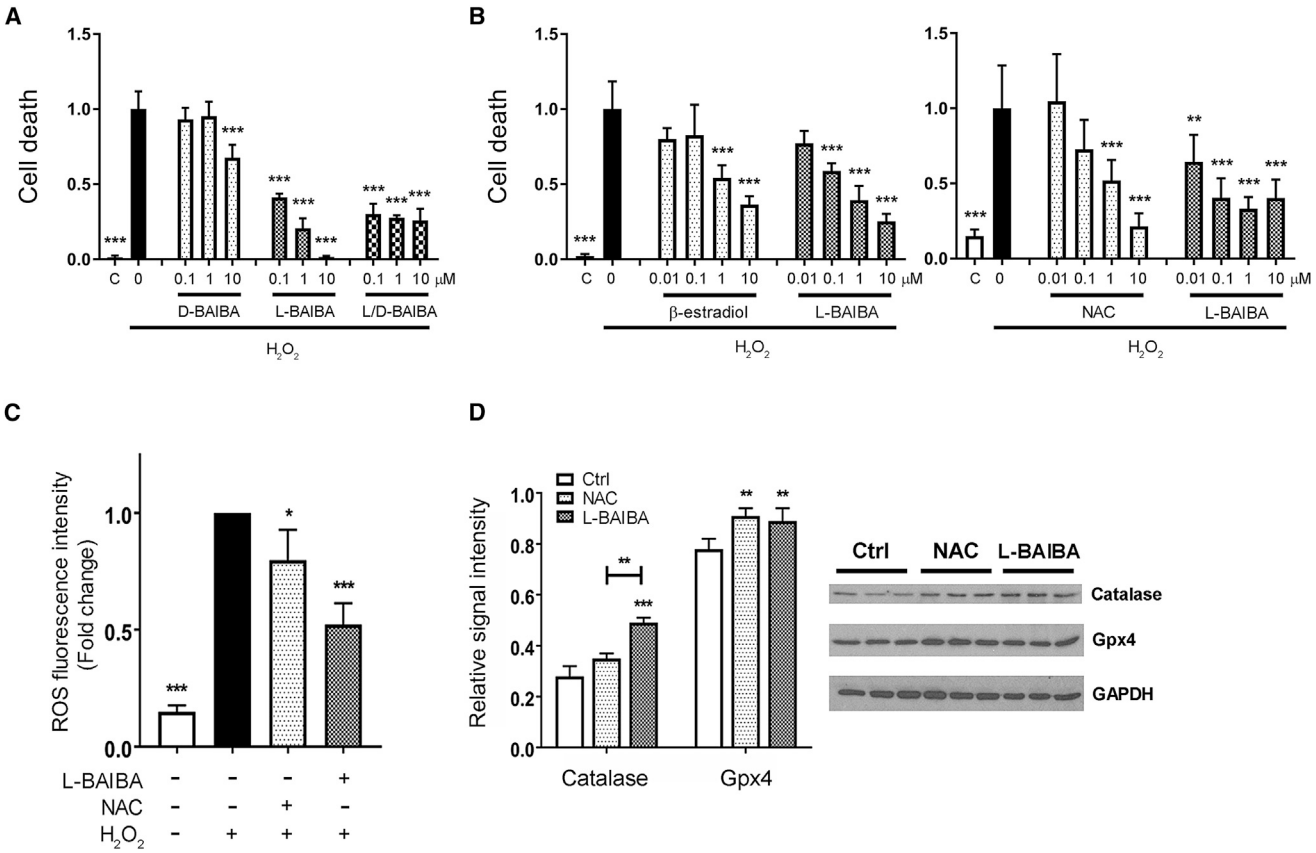

Figure 1. L-BAIBA Protects Osteocytes from Cell Death Induced by Oxidative Stress

(A) Cell death assay using the osteocyte cell line MLO-Y4. L-BAIBA as well as L/D-BAIBA, but not D-BAIBA, showed highly significant protective effects on MLO-Y4 cell death induced by oxidative stress. ***$p < 0.001$ versus H_2O_2.

(B) Comparison of potency between L-BAIBA and well-known antioxidants β-estradiol and N-acetylcysteine (NAC) on MLO-Y4 cell death induced by oxidative stress. **$p < 0.01$ and ***$p < 0.001$ versus H_2O_2.

(C) Prevention by L-BAIBA of reactive oxygen species (ROS) generation induced by oxidative stress. *$p < 0.05$ and ***$p < 0.001$ versus H_2O_2.

(D) Induction of antioxidant enzymes, catalase, and Gpx4 by L-BAIBA. **$p < 0.01$ and ***$p < 0.001$ versus control.

The data are expressed as the mean ± SD. See also Figures S1–S3.

significantly higher bone volume fraction (BV/TV), and higher thickness and connectivity of trabecular bones compared to control group that was gender-independent (Figures 2A–2E). *Ex vivo* μCT analysis confirmed the *in vivo* μCT data (Figures 2F–2J). EF analysis revealed more plate-type-dominated structures retained in males after 2-week hindlimb unloading, while bone in the control group shifted to more intermediate structures. No differences in EF analysis in female mice were observed (Figures 2K–2N). By histological analysis, bone parameters were generally consistent with μCT data as shown in Figure 2, and, while there was no effect on osteoclast parameters in both males and females, osteoblast number and surface were significantly higher in male L-BAIBA-treated animals (Figures 3A–3H). Similar to the *ex vivo* μCT data shown in Figure 2, there was a significant difference, higher BV/TV, trabecular number (Tb.N), and trabecular thickness (Tb.Th.) and lower trabecular separation (Tb.Sp.), in treated compared to control males. Unlike the μCT data in Figure 2, no significant differences were observed in bone parameters in females. Significantly greater apoptosis was observed in osteocytes in the untreated as compared to the L-BAIBA-treated animals (Figure 3I). Real-time PCR did not show a significant change in *Rankl*, *Opg*, and *Sost* mRNA obtained from femurs (Figure 3J).

To determine if the administration of L-BAIBA has an additional effect on muscle function in the disuse model, *ex vivo* contractility of the EDL (mainly consisting of glycolytic muscle fibers) and of the soleus (mainly consisting of oxidative muscle fibers) muscles was performed. EDL showed significantly greater muscle mass and maximal tetanic force in male mice receiving L-BAIBA over controls (Figures 4A and 4B). A significant difference in soleus half-maximal force and rate of force development was observed in L-BAIBA-treated males (Figures 4H and 4J). Additionally, the force-frequency relationship of soleus from male mice treated with L-BAIBA showed higher relative forces at stimulatory frequencies in the range of 40–80 Hz compared to non-treated controls (Figure 4L). Interestingly, EDL and soleus muscles from female mice were virtually unaffected by L-BAIBA treatment (Figures 4A–4L).

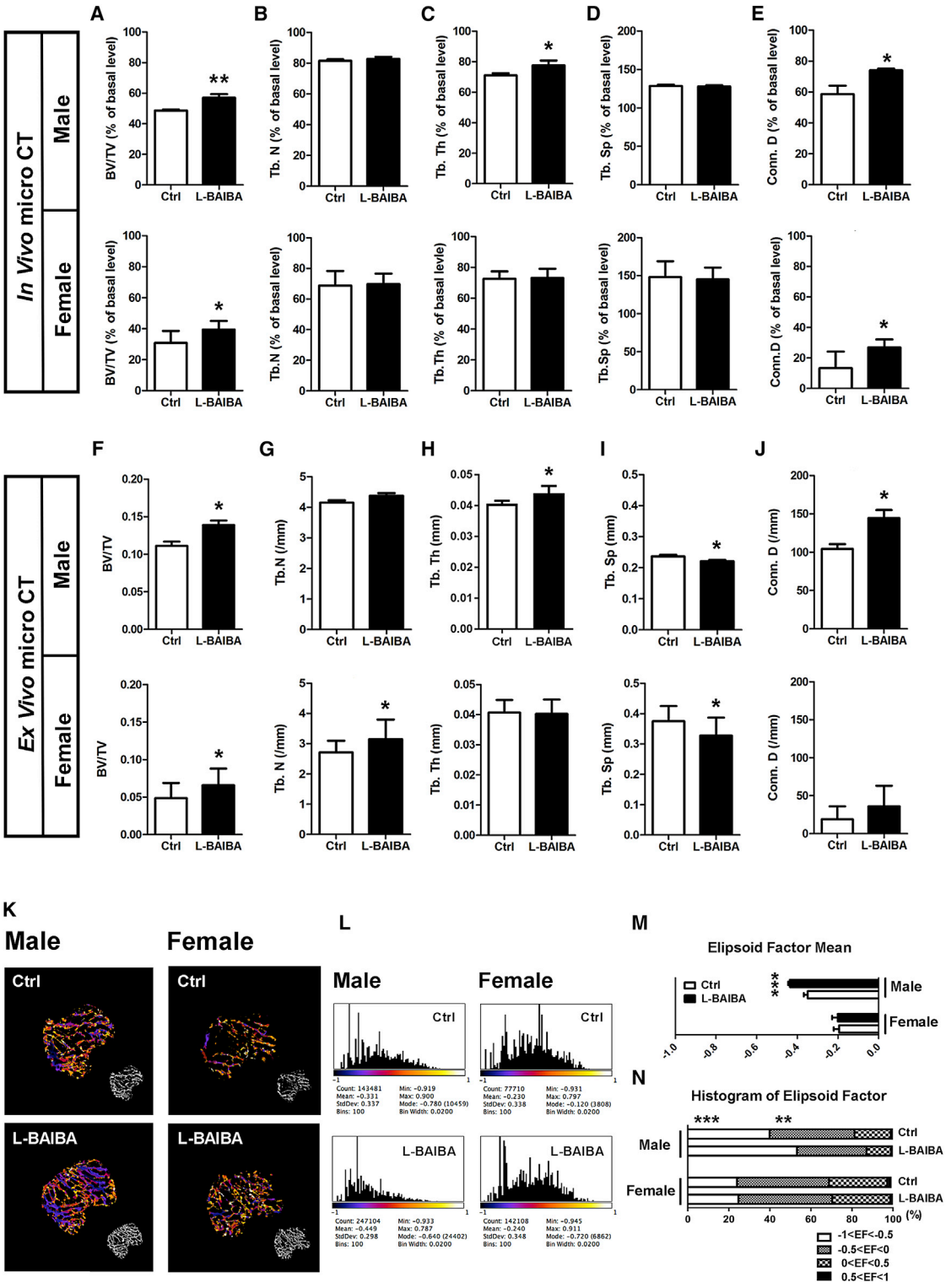

Figure 2. L-BAIBA Maintains Trabecular Bone Mass and Connectivity after 2 Weeks of Hindlimb Unloading

(A–J) μCT analysis of cancellous bones in right proximal tibiae, *in vivo* (A–E) and *ex vivo* (F–J). Bone volume fraction (BV/TV) (A and F), trabecular number (Tb.N) (B and G), trabecular thickness (Tb.Th) (C and H), trabecular separation (Tb.Sp) (D and I), and connectivity density (Conn.D) (E and J) were examined. Upper panel is for the 5-month-old male (n = 6) and lower panel is for the 3-month-old female (n = 6). All the parameters *in vivo* μCT are expressed as a percentage of baseline. *p < 0.05 and **p < 0.01 versus control.

(legend continued on next page)

L-BAIBA Is Produced by Both Young and Old Contracted Muscle

To determine if BAIBA is produced by both young and aged muscle, CM were obtained from both EDL and soleus muscles dissected from male and female mice, 5 and 22 months old, with and without contraction at 90 Hz. Muscle CM were freeze-dried, derivatized using Marfey's reagent, and then quantitated by liquid chromatography-mass spectrometry (LC-MS) as described previously (Vemula et al., 2017). Contraction stimulated L-BAIBA production in all muscle, EDL and soleus, male and female, but to a greater extent in aged muscle compared with young muscle (Figure 5A). There were no significant changes in 20 amino acids or in the BAIBA analogs, such as γ-aminobutyric acid (GABA) (Figures S4A and S4B).

L-BAIBA Protects Young, but Not Old, Osteocytes from ROS-Induced Cell Death

To begin to determine if BAIBA might function as an osteocyte-protective agent with aging, osteocytes from both 5- and 22-month-old male and female mice were tested. L/D-BAIBA and L-BAIBA blocked the negative effects of ROS on young, but not old, osteocytes (Figures 5B and 5C).

L-BAIBA Signals through the MRGPRD to Protect Osteocytes from Cell Death

As old muscle was just as capable as young muscle to secrete L-BAIBA in response to contraction, we asked if the receptor for BAIBA could be affected by aging. Mas-related G protein-coupled receptor type D (*Mrgprd*) and glycine receptors, both known BAIBA receptors, were examined in primary bone cells. The *Mrgprd* was highly expressed in primary osteocytes especially at 5 months of age (Figure 6A). Expression increased from 2.5 months to 5 months and highly decreased by 22 months of age. The expression level was higher in males compared to females. These receptors were more highly expressed in the primary osteocyte population compared to primary osteoblasts (Figure 6A). Glycine receptors (*Glra4* and *Glrb*) were expressed at lower levels than the *Mrgprd* (Figure 6B). Even though the *Glrb* was highly expressed in MLO-Y4 cells, there was a little expression of its potential subunit, *Glra4*, that was dimerized to form their functional receptor (Figure 6C). *Glra1–3* were not detectable. Other ligands for these receptors include β-alanine and GABA, so these were compared to L-BAIBA for osteocyte-protective capacity. L-BAIBA was approximately 100-fold more potent than β-alanine, GABA, or glycine (Figure 6D). To determine if MRGPRD is the functional receptor for BAIBA, inhibitory assays were performed. The receptor antagonist for MRGPRD, MU6840, significantly attenuated the activity of L-BAIBA (Figure 6E). Experiments were performed using small interfering RNA (siRNA) and CRISPR technology for knockdown studies. *Mrgprd*-targeted siRNA was shown to completely block the expression of mRNA (Figure 6F) and reverse the positive effects of L-BAIBA on H_2O_2-induced cell death (Figure 6G). Two different *Mrgprd* single guide RNAs (sgRNAs) were shown to significantly reduce protein expression of MRGPRD (Figure 6H) and to significantly block the positive effects of L-BAIBA on H_2O_2-induced cell death (Figure 6I). Therefore, based on inhibitor and knockdown studies, the MRGPRD appears to be the receptor mediating the protective effects of L-BAIBA on osteocytes.

Mitochondria Movement and Dynamics in Osteocytes

Next, we asked how L-BAIBA maintains osteocyte viability. Osteocytes have been imaged previously *in vivo* for active mitochondria using Tetramethylrhodamine, ethyl ester, *TMRE*, a cell-permeant, cationic, red-orange fluorescent dye that is readily sequestered by active mitochondria (Frikha-Benayed et al., 2016). These investigators suggested that osteocytes with impaired mitochondrial function may be more susceptible to apoptosis. As mitochondria are known to produce ROS as a by-product along with the production of ATP, we decided to determine if mitochondria might be involved in the protective effects of BAIBA on H_2O_2-induced cell death. Using Mito Red, we found that mitochondria can be imaged over time in MLO-Y4 cells and mitochondria can be observed moving in the dendritic processes, similar to that observed with oligodendrocyte primary processes and neuronal dendrites (Rinholm et al., 2016) (Figure 7A; Movies S1 and S2). Primary osteocytes isolated from Dmp1-GFP mice showed similar properties with regard to mitochondrial movement (Figure 7A; Movie S3).

L-BAIBA Prevents Mitochondrial Breakdown due to ROS

To determine if L-BAIBA would prevent the negative effects of ROS on mitochondria, time-lapse imaging experiments were performed. When H_2O_2 (100 μM) was applied to MLO-Y4 osteocyte-like cells, unopposed fission occurred over 50 min along with reduced TMRE intensity (Figure 7B), but this effect was blocked by L-BAIBA (Figures 7C and 7D). To quantitate the mitochondrial functional status, cells were stained with TMRE, which is fluorescent only in functional mitochondria, and with mitoD, which stays fluorescent whether the mitochondria are functional or not. The ratio of TMRE/mitoD, which is related to mitochondrial membrane potential, is shown in Figures 7E–7G. This ratio was significantly reduced with H_2O_2, while L-BAIBA pretreatment maintained the same ratio in response to H_2O_2 as non-treated cells. Therefore, L-BAIBA appears to protect osteocytes through the maintenance of their mitochondria. Not only does L-BAIBA have short-term effects on mitochondria integrity but also it regulates mitochondrial gene expression (Figure S5).

DISCUSSION

The effects of muscle on bone were previously thought to be exclusively mediated through mechanical loading, however, here we show that, in addition, the muscle can have effects on

(K–N) Ellipsoid factor (EF) classification for rod/plate geometry. Representative 3D color map images of control and L-BAIBA (K) indicate EF > 0 in orange-yellow (rod type) and EF < 0 in purple-blue (plate type). Corresponding EF histograms of control and L-BAIBA (L) indicate a shift to the left for plate-dominated structures and to the right for rod-dominated structures. Mean of EF (M) and summary of EF histograms (N) are shown. 5-month-old male, n = 6; 3-month-old female, n = 6. **p < 0.01 and ***p < 0.001 versus control.
The data are expressed as the mean ± SD.

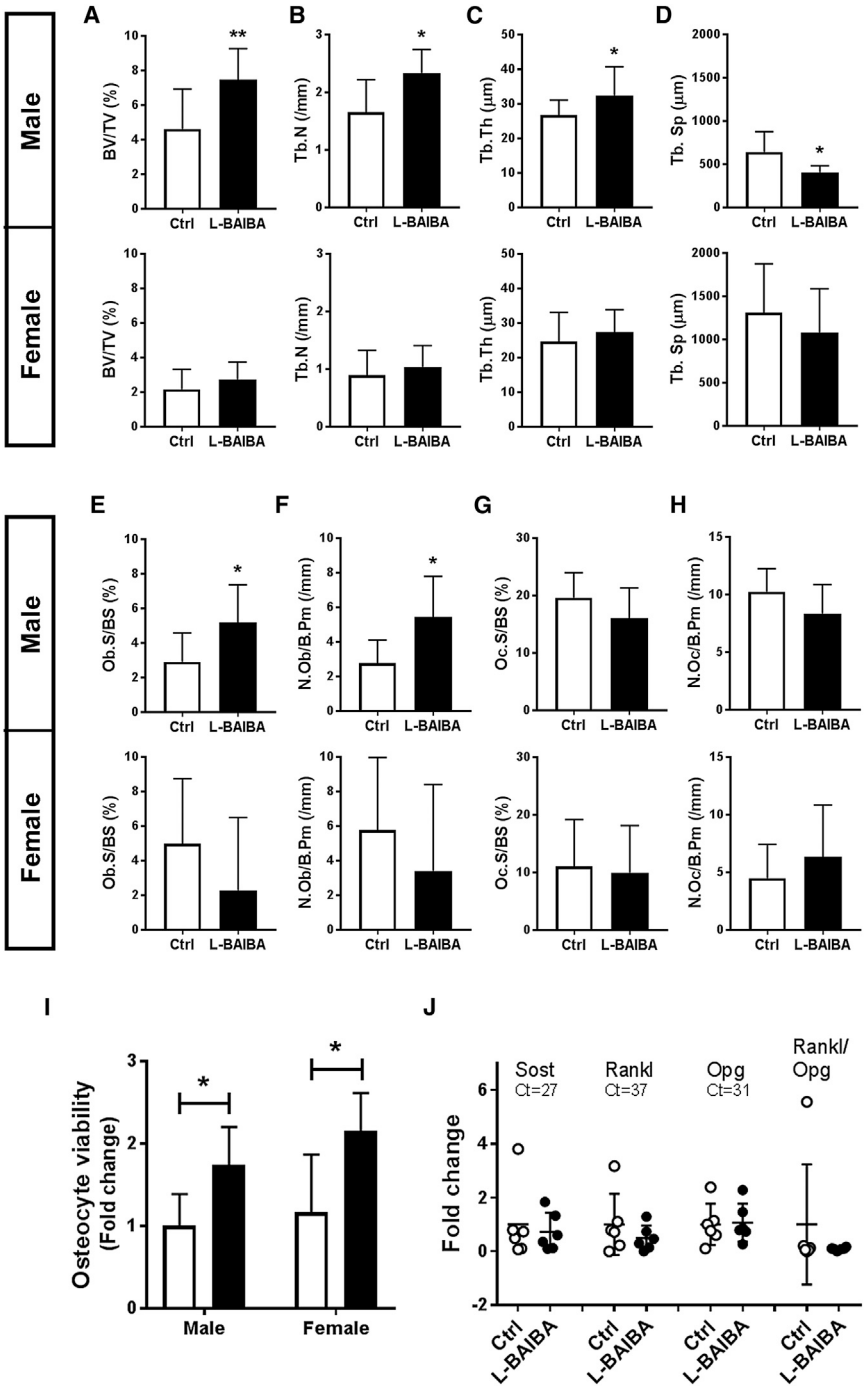

Figure 3. L-BAIBA Maintains Trabecular Bone Mass and Osteocyte Viability after 2 Weeks of Hindlimb Unloading

(A–H) Bone static histomorphometry of cancellous bones in left proximal tibiae, *in vivo*. Bone volume fraction (BV/TV) (A), trabecular number (Tb.N) (B), trabecular thickness (Tb.Th) (C), trabecular separation (Tb.Sp) (D), osteoblast surface (Ob.S/BS) (E), osteoblast number (N.Ob/B.Pm) (F), osteoclast surface (Oc.S/BS) (G), and osteoclast number (N.Oc/B.Pm) (H) were examined. Upper panel is for the 5-month-old male (n = 6) and lower panel is for the 3-month-old female (n = 6). *p < 0.05 and **p < 0.01 versus control.

(I) Osteocyte viability evaluated by TUNEL apoptosis assay with 5-month-old male (n = 6) and 3-month-old female (n = 6). *p < 0.05 versus control.

(J) Real-time qPCR analysis of Sost, Rankl, and Opg mRNA expression in femurs obtained from hindlimb unloaded male mice (n = 6). Data are expressed as fold change over the expression level of each gene in control mice (average Ct value is 27 for Sost, 37 for Rankl, and 31 for Opg). No significant difference was detected compared to control.

The data are expressed as the mean ± SD.

bone through a secreted metabolite, BAIBA. Others have shown that muscle can secrete factors that have effects on other tissues. Originally these factors were termed myokines and shown to be secreted proteins (Pedersen, 2011). Exercise has been shown to stimulate skeletal muscle to secrete soluble factors that modulate bone metabolism, such as IGF-1 and FGF-2 (Hamrick et al., 2010) and irisin, which has been shown to increase bone mass (Colaianni et al., 2015). We proposed that muscle would secrete proteins that would protect osteocytes from cell death (Jähn et al., 2012), but we found a small molecular weight molecule, a metabolite, was responsible. Both the slow-twitch oxidative muscle, such as soleus, and fast-twitch glycolytic muscles, such as EDL, secrete BAIBA when contracted. BAIBA was found to be as or more potent than known protective factors β-estradiol and NAC.

BAIBA is a small molecule produced by skeletal muscle during exercise (Roberts et al., 2014). BAIBA consists of two enantiomers, L-BAIBA and D-BAIBA. This non-protein β-amino acid, L-BAIBA, is produced from the utilization of a branched amino acid L-valine as an energy source under the control of transcriptional co-activator PGC-1α. BAIBA was shown to be a mediator of the beneficial effect of exercise from skeletal muscle to other tissue organs in an endocrine manner. It activates the β-oxidation pathway of hepatic fatty acid, and it triggers the browning of white adipose tissue (Roberts et al., 2014), improves insulin resistance and inflammation in skeletal muscle in an autocrine/paracrine manner (Jung et al., 2015), prevents diet-induced obesity (Begriche et al., 2008), and protects against metabolic disturbance in type 2 diabetes (Shi et al., 2016). We have now shown another function for this muscle metabolite, that of protecting osteocytes from cell

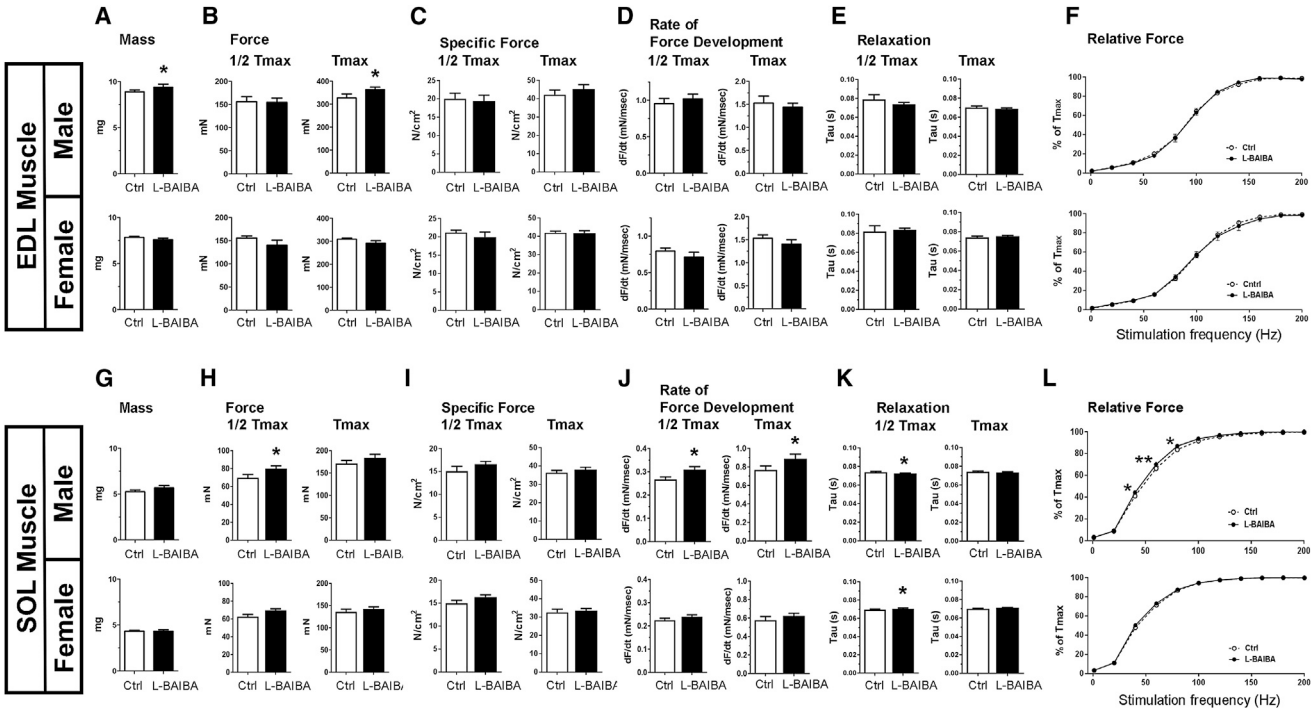

Figure 4. L-BAIBA Maintains EDL and Soleus Muscle Function after 2 Weeks of Hindlimb Unloading

(A–L) EDL and soleus muscle functional analysis, EDL (A–F) and soleus (G–L). Half-maximal (1/2 Tmax) and maximal tetanic contractions (Tmax) are shown in left and right panels, respectively. Upper panel is for the 5-month-old male (n = 6) and lower panel is for the 3-month-old female (n = 6). Muscle mass (A and G), muscle force (B and H), muscle-specific force (C and I), muscle rate of contractile force development (D and J), muscle relaxation (E and K), and muscle relative force (F and L) are examined. Relative force is a force versus frequency relationship among the stimulatory frequencies of 1–200 Hz, wherein force at each frequency is expressed as a percentage of Tmax. *$p < 0.05$ and **$p < 0.01$ versus control.

The data are expressed as the mean ± SD.

death. *In vivo*, this metabolite retains bone and muscle with unloading apparently through this mechanism.

Every amino acid except glycine has two enantiomers. Usually naturally occurring amino acids in cells are the L-form, not the D-form. However, D-BAIBA is derived from thymine and excluded in the urine (Smith and Dymond, 1963). We determined the greater potency of the L-form compared to the D-form on osteocyte viability (Figure 1A). We have also shown that L-BAIBA, but not D-BAIBA, is produced by contracted muscle regardless of skeletal muscle type, gender, and age (Figure 5A). As far as we know, the different enantiomers have not been tested on the MRGPRD signaling, but, based on our results, it is assumed that the L-form is the biologically active form that binds to this receptor.

Osteocytes are one of the longest-lived cells in the body, remaining viable in the bone matrix for decades (Manolagas and Parfitt, 2013). Osteocyte viability is crucial for the normal functioning of the skeleton and potentially for the normal function of other organs, such as kidney and muscle. Osteocytes are multifunctional cells that regulate bone remodeling through osteoblasts and osteoclasts, act as endocrine cells targeting other tissues, regulate both calcium and phosphate homeostasis, and also act as mechanosensory cells that signal for bone removal with disuse and bone formation with anabolic loading (Bonewald, 2011; Dallas et al., 2013).

Programmed osteocyte cell death is necessary to repair damaged bone (Kennedy et al., 2012; Verborgt et al., 2000, 2002). This type of osteocyte cell death acts as a beacon to direct osteoclasts to the microdamaged bone for removal as the osteocytes sacrifice themselves in order to repair bone. This process is highly programmed to release factors, such as RANKL, to direct osteoclasts to damaged sites for repair. Therefore, it is important to maintain the health and function of the osteocyte to maintain bone homeostasis. However, as we age, these cells begin to die and their remains are removed and lost through the lacuno-canalicular system, leaving empty lacunae, or the dying cells can vesiculate and micropetrose, resulting in a mineralized filling in of their lacunae (for reviews on osteocytes, see Bonewald, 2011 and Dallas et al., 2013). This results in a compromised lacuno-canalicular system with impaired osteocyte signaling.

BAIBA was reported to bind to glycine receptors and to the MRGPRD, which is also known to be a receptor for β-alanine, and the neurotransmitter GABA (Uno et al., 2012). The *Mrgprd* is most highly expressed in nonpeptidergic dorsal root ganglia neurons (Zylka et al., 2005) and found to be the sensory receptor for irritation, such as noxious mechanical stimuli (Cavanaugh et al., 2009). Protein expression was only found in dorsal root ganglia (McNeil and Dong, 2014), but low mRNA levels were detected in bladder, uterus, testes, arteries, and femur

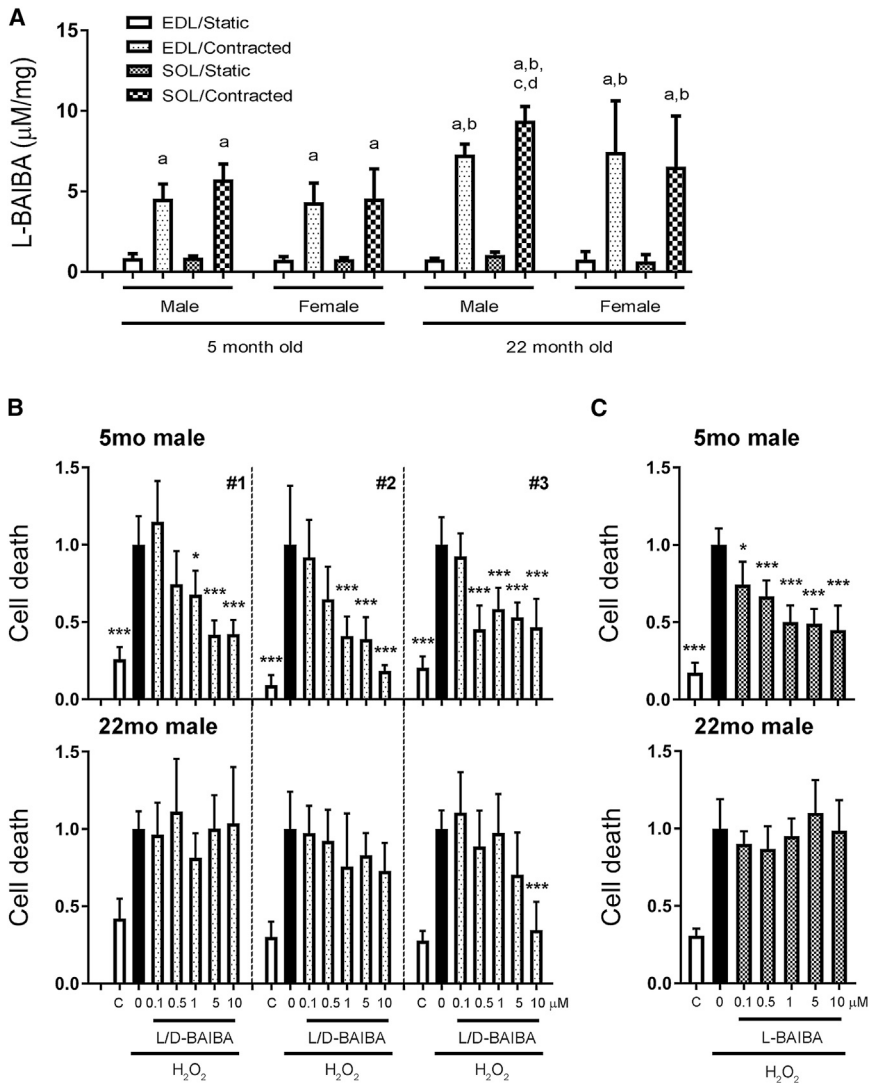

Figure 5. L-BAIBA Is Secreted by Both Young and Old Contracted Muscle but Only Protects Young, but Not Old, Primary Osteocytes from Cell Death Induced by Oxidative Stress

(A) L-BAIBA production by *ex vivo* contracted muscle at 90 Hz. The amount of L-BAIBA was normalized by muscle mass. a, versus corresponding non-contracted muscle CM; b, versus corresponding contracted muscle CM obtained from 5-month-old mice; c, versus corresponding contracted muscle CM obtained from female mice; d, versus contracted EDL muscle CM obtained from 22-month-old male mice; $p < 0.05$.

(B and C) Cell death assay of primary bone cells from long bones. L/D-BAIBA (B) and L-BAIBA (C) protect primary bone cells obtained from 5-month-old male mice (upper panel) under oxidative stress, but not the ones from 22-month-old male mice (lower panel). *$p < 0.05$ and ***$p < 0.001$ versus H_2O_2.

The data are expressed as the mean ± SD. See also Figure S4.

(Shinohara et al., 2004). We found that an MRGPRD antagonist, MU6840 (Uno et al., 2012), blocked the beneficial effect of L-BAIBA ROS-induced cell death, as did both siRNA and sgRNA to *Mrgprd*. Whereas muscle from both young, 5-month-old, and 22-month-old mice produce BAIBA in response to contraction, osteocytes from old mice are not protected by BAIBA to the same extent as young osteocytes. *Mrgprd* was highly expressed in young osteocytes but decreased in expression in old osteocytes. This suggests that osteocytes lose their response to BAIBA with aging. Aged contracted muscle can produce BAIBA in response to exercise, but the reduction in receptor expression may reduce the beneficial effects of exercise on osteocytes.

A number of factors have been shown to induce osteocyte cell death, including glucocorticoids and cytokines such as IL-1 and TNF-α. Conversely, a number of molecules have been shown to protect osteocytes from cell death, including estrogen and bisphosphonates (for review, see Bellido and Plotkin, 2011; Jilka et al., 2013; Jilka and O'Brien, 2016). We showed that secreted muscle factors could protect osteocytes from glucocorticoid-induced cell death and that this effect was mediated through the β-catenin-signaling pathway (Jähn et al., 2012). It has been suggested that oxidative stress caused by disuse, estrogen deficiency, excess corticosterone, and aging may be responsible for bone cell death and, therefore, bone fragility (Almeida and O'Brien, 2013). Here we performed studies examining the effects of ROS, known to be generated with aging, on osteocyte viability. Mitochondria play a crucial role in cell survival. Mitochondria require ROS for normal function (Holzerová and Prokisch, 2015), but with aging excess ROS leads to mitochondrial breakdown (Finkel, 2015; Valko et al., 2007). During apoptosis, alteration of mitochondrial structure and reduction of membrane potential are present. Mitochondria show massive fragmentation of their network associated with cytochrome *c* release, which induces the formation of the apoptosome leading to activation of caspase-3, responsible for apoptosis (Langlais et al., 2015). We were able to image mitochondria in both MLO-Y4 cells and primary osteocytes, showing trafficking similar to that observed in axonal neural cells (Rinholm et al., 2016). Here we show that BAIBA prevented or reduced this massive breakdown of mitochondria induced by H_2O_2 in MLO-Y4 osteocyte-like cells.

As BAIBA production is increased with exercise (Roberts et al., 2014) and with contraction of isolated EDL and soleus as shown in this study, the hindlimb unloading assay, a model of disuse or lack of exercise, was performed to determine the effects of L-BAIBA on both bone and muscle. The detrimental effects of unloading on bone mass through osteocytes are well described (Basso and Heersche, 2006), and it has previously been shown

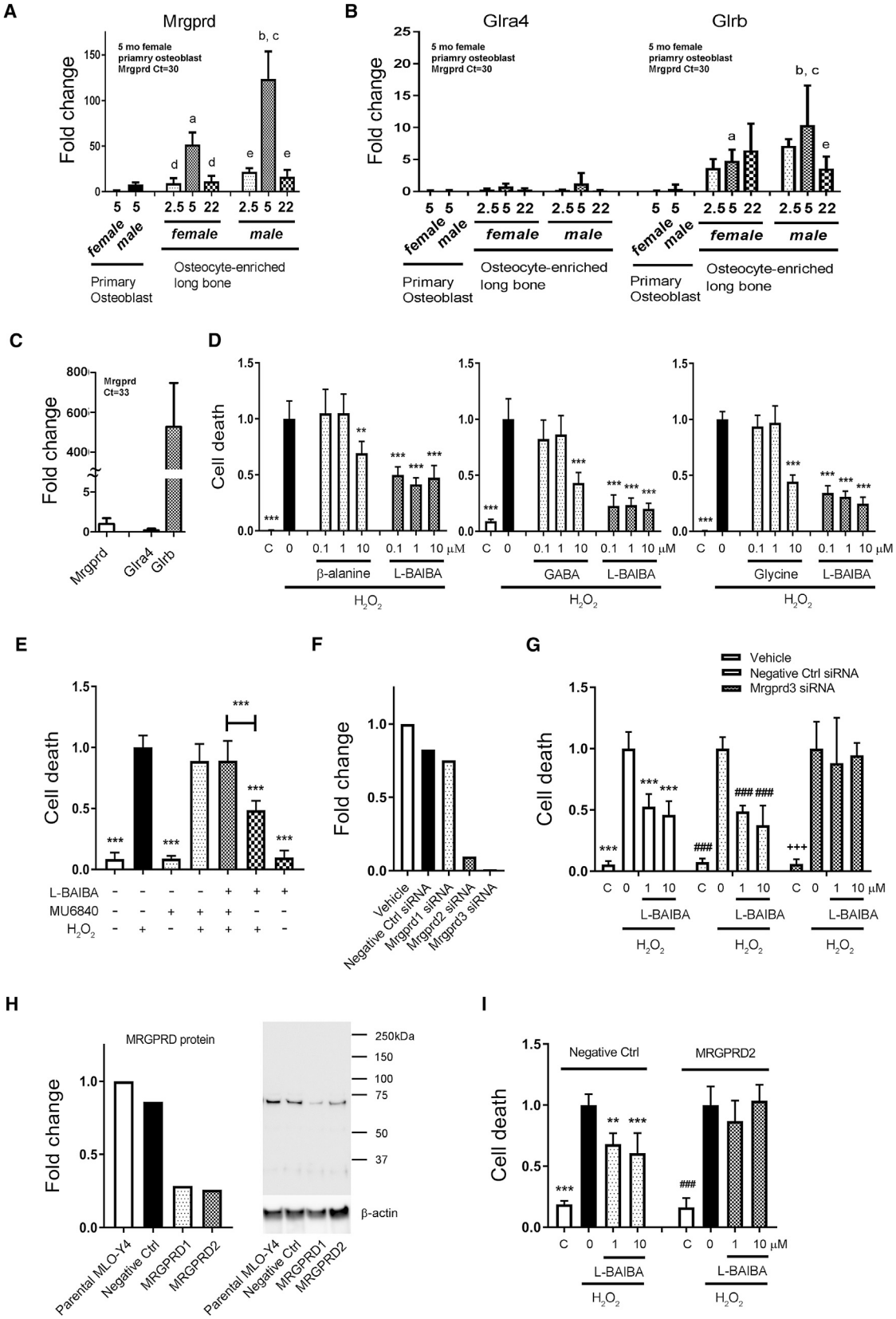

(legend on next page)

that blocking osteocyte apoptosis prevents bone loss due to hindlimb unloading (Cabahug-Zuckerman et al., 2016). We found that providing L-BAIBA in drinking water for 2 weeks of hindlimb unloading retained bone mass, more so in males than females, most likely due to the greater amount of trabecular bone in males compared to females even with using 3-month-old females as compared to 5-month-old males. By histomorphometric analysis, more bone was retained in males given L-BAIBA, but this was not observed in females, most likely due to the low amount of trabecular bone, which can be more easily quantitated using 3-dimensional μCT, but not 2-dimensional bone histomorphometry. Also, significantly greater apoptosis was observed in osteocytes in the untreated as compared to the L-BAIBA-treated animals, whereas no differences were observed in mRNA for the osteocyte factors, sclerostin, Rankl, or osteoprotegerin. These data suggest that L-BAIBA protects both osteoblasts and osteocytes through maintenance of viability and not through regulation of osteoblasts via sclerostin and osteoclasts via Rankl/Opg. L-BAIBA could potentially be exerting a direct effect on osteoblasts, but, as osteocytes express much higher levels of *Mrgprd*, the effects on osteoblasts could be indirect through the maintenance of osteocyte viability.

Male mice treated with L-BAIBA during hindlimb unloading retained EDL muscle mass and maximal contractile force over controls, however, EDL maximal force normalized to muscle size was similar between groups, indicating that the higher EDL mass in the L-BAIBA-treated group accounted for the higher contractile force. Soleus muscles from L-BAIBA-treated mice displayed higher contractile force and rate of force development at stimulatory frequency, which produces approximately half of maximal contractile force output (40 Hz) as well as a leftward shift in the force-frequency curve at 40–80 Hz over controls. The force-frequency profile is indicative of muscle fiber myosin heavy chain (MHC) composition, with slow type 1 muscle fibers displaying higher Ca^{2+} sensitivity as well as the higher rates of calcium sarcoplasmic reticulum (SR) release at these lower frequencies of stimulation and, therefore, higher relative forces at suboptimal frequencies compared to fast type 2 MHC-enriched muscle fibers. Enhanced muscle contractility at these lower frequencies is very physiologically relevant, especially when considering that mammalian skeletal muscles normally function in this range (Edwards et al., 1977a, 1977b). These studies also demonstrate that muscle mass does not necessarily directly correlate with function, therefore, function can be preserved despite no gains in muscle mass. Interestingly, EDL and soleus muscles from female mice were virtually unaffected by L-BAIBA treatment. These differences in response to L-BAIBA could be due to the combined effects of higher estrogen expression levels and lower testosterone concentrations in combination with the higher docosahexaenoic acid (DHA) in the female's body, as observed in humans (Bakewell et al., 2006; Giltay et al., 2004).

Based on these observations, one might speculate that BAIBA may exert not only direct effects on bone cells but also indirect effects by preserving muscle that directly loads the tibia, especially in male mice. Retention or preservation of both mechanical stimuli and secreted myokines such as BAIBA may act together to preserve bone mass. In the EDL muscle composed of different muscle fiber types, L-BAIBA may be acting through preservation of muscle mass. Muscle disuse is known to lead to shifts in MHC expression from slow MHC type 1 to faster MHC type 2 isoforms in slow-twitch muscles like the soleus. BAIBA has been found to induce expression of peroxisome proliferator-activated receptor delta (PPARδ) in skeletal muscle (Jung et al., 2015), a known regulator of slow type 1 muscle fiber development/maintenance (Ehrenborg and Krook, 2009). This suggests that L-BAIBA may attenuate disuse-induced fiber type switching in soleus muscle via the induction of PPARδ expression. The autocrine effects of BAIBA on muscle will require additional investigation, especially in the context of bone and muscle crosstalk.

In summary, we have identified another function for the muscle-derived metabolite L-BAIBA on osteocyte viability. L-BAIBA protects osteocytes from ROS-induced apoptosis through the MRGPRD and through maintaining mitochondria integrity. This protective capacity appears lost with aging due to the downregulation of *Mrgprd* expression in osteocytes. Therefore, targeting receptor expression in osteocytes with aging may return the bone anabolic response to exercise.

Figure 6. The Protective Effects of L-BAIBA on Osteocyte Viability Are Mediated through the MRGPRD

(A and B) Real-time qPCR analysis of *Mrgprd* (A) and Glra4/b (B) mRNA expression in primary osteoblast fractions and osteocyte-enriched bones obtained from male and female at 2.5, 5, and 22 months old. Data are expressed as fold change over the *Mrgprd* expression level in primary osteoblast fractions obtained from 5-month-old female mice (average Ct value is 30). *Glra1–3* are undetectable. a, versus 5-month-old female primary osteoblast fraction (pObF); b, versus 5-month-old male pObF; c, versus 5-month-old female osteocyte-enriched bones (pOcyB); d, versus 5-month-old female pOcyB; e, versus 5-month-old male pOcyB; $p < 0.05$.

(C) Real-time qPCR analysis of *Mrgprd* and *Glra4/b* mRNA expression in MLO-Y4 cells. Data are expressed as fold change over the *Mrgprd* expression level (average Ct value is 33). *Glra1–3* are undetectable.

(D) Comparison of L-BAIBA with other MRGPRD ligands, β-alanine, GABA, and glycine in cell death assay. $^{**}p < 0.01$ and $^{***}p < 0.001$ versus H_2O_2.

(E) An antagonist against MRGPRD, MU6840 prevents the protective effect of L-BAIBA on osteocyte viability. $^{***}p < 0.001$ versus H_2O_2.

(F) Real-time qPCR analysis to determine the efficiency of *Mrgprd* knockdown using RNAi system. Data are expressed as fold change over the expression level in parental MLO-Y4.

(G) *Mrgprd* knockdown by siRNA prevents the protective effect of L-BAIBA on osteocyte viability. $^{***}p < 0.001$ versus vehicle/H_2O_2, ###$p < 0.001$ versus negative control/H_2O_2, and +++$p < 0.001$ versus *Mrgprd* siRNA/H_2O_2.

(H) Western blot analysis to determine the efficiency of *Mrgprd* knockout using CRISPR/Cas9 system. Data are normalized by β-actin and expressed as fold change over the expression level in parental MLO-Y4.

(I) *Mrgprd* knockout by CRISPR/Cas9 prevents the protective effect of L-BAIBA on osteocyte viability. $^{**}p < 0.01$ and $^{***}p < 0.001$ versus negative control/H_2O_2 and ###$p < 0.001$ versus MRGPRD2/H_2O_2.

The data are expressed as the mean ± SD.

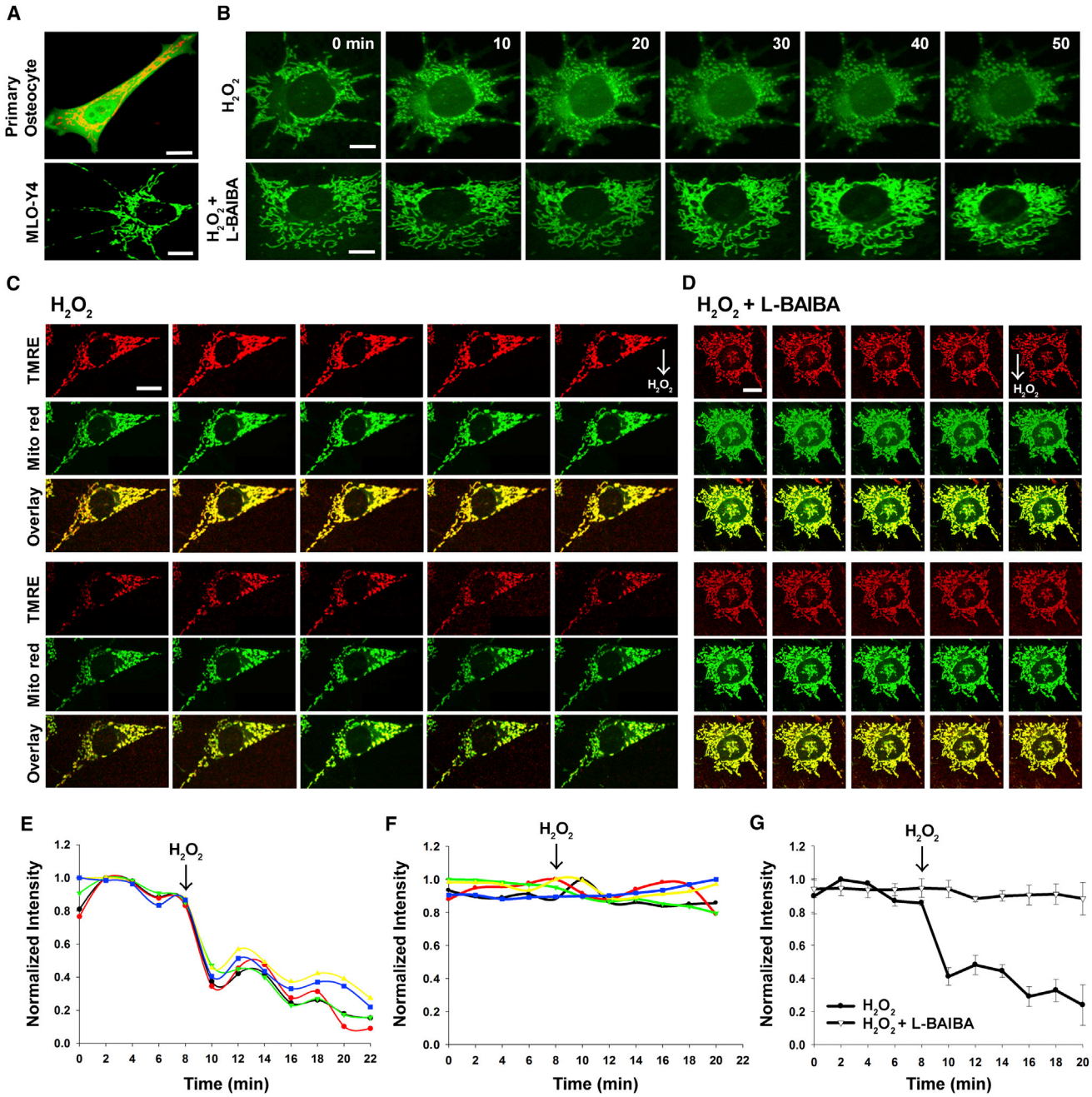

Figure 7. Confocal Microscopy Images of Mitochondrial Response to Acute Treatment of Hydrogen Peroxide in Live Cells, Prevention of Mitochondrial Breakdown by L-BAIBA

(A) Mitochondria in a primary osteocyte (top) and a MLO-Y4 cell (bottom).

(B) Time-lapse confocal imaging of mitochondria in MLO-Y4 cell after treatment with hydrogen peroxide (100 μM) alone (top row) and with 100 μM hydrogen peroxide plus L-BAIBA (bottom row).

(C and D) Evaluation of mitochondrial membrane potential using TMRE (red) and structure using Mito Red (green) with the treatment of hydrogen peroxide alone (C) and of hydrogen peroxide plus L-BAIBA (D). Arrow indicates the time that hydrogen peroxide was added.

(E–G) Quantification of the change of fluorescent intensity (TMRE) over the time per cell before and after treating with hydrogen peroxide (E), hydrogen peroxide plus L-BAIBA (F), and average fluorescence intensity of TMRE (n = 5) (G). Arrow indicates the time that hydrogen peroxide was added. Scale bar, 10 μm. See also Figure S5.

EXPERIMENTAL PROCEDURES

Please refer to the Supplemental Experimental Procedures for a detailed description of other experiments.

MLO-Y4 Cells

The osteocyte-like MLO-Y4 cell line, derived from murine long bone, was used as an *in vitro* osteocyte model (Kato et al., 1997). MLO-Y4 cells were maintained on collagen type I-coated plates in α-MEM supplemented with 2.5% fetal bovine serum (FBS), 2.5% calf serum (CS), and 100 U/mL penicillin/streptomycin (P/S) in a 5% CO_2 incubator at 37°C. For all assays, phenol red-free α-MEM was used.

Isolation of Primary Bone Cells from Mouse Long Bones

Primary bone cells were isolated as previously described with some modifications (Stern et al., 2012). Briefly, long bones were dissected from 5- or 22-month-old C57BL/6 male mice for cell death assay and from 3-month-old DMP1-GFP female mice for live imaging. After removal of soft tissue, epiphyses were cut off and bones were flushed with PBS using a 27G½ needle-syringe to remove bone marrow. Bones were then longitudinally cut and digested 3 times with 300 U/mL collagenase type IA (Sigma-Aldrich, C9891), one time with 5 mM EDTA (Sigma-Aldrich, E5134)/0.1% BSA (Sigma-Aldrich, A7030), and one more with the collagenase, each for 25 min at 37°C. The bones were minced into small pieces and cultured in 5% FBS/5% CS/α-MEM in a 6-well plate coated with 0.15 mg/mL rat tail collagen type I (Corning, 354236) until primary bone cells were obtained as an outgrowth from the bone chips.

Quantification of Cell Death

MLO-Y4 cells or primary bone cells obtained from long bones were plated at $1–1.25 \times 10^4/cm^2$ on a collagen-coated 96-well plate with 6 wells for each experimental condition. Representative examples of two or four independent experiments are shown. Cells were pretreated with varying concentrations of L/D-BAIBA (Sigma-Aldrich, 217794), L-BAIBA (Sigma-Aldrich, 51511), D-BAIBA (Sigma-Aldrich, 68337), β-estradiol (Sigma-Aldrich, E8875), NAC (Sigma-Aldrich, A7250), β-alanine (Sigma-Aldrich, 146064), or GABA (Sigma-Aldrich, A2129) in 1% FBS/1% CS/α-MEM for 1 or 24 hr, followed by treatment with 0.3 mM hydrogen peroxide (EMD Millipore, HX0635-3) for 3–4 hr in 0.5% FBS/0.5% CS/α-MEM to induce 20%–40% cell death. The cells were pretreated with MU6840 (Key Organics, 5R-0328) for 30 min before adding L-BAIBA. Cells were stained with 2 μM ethidium homodimer 1 (EthD-1, Invitrogen, E1169) for 30 min and analyzed on a Nikon Eclipse TE300 inverted fluorescence microscope to detect dead cells. Images were acquired under 10× magnification using epifluorescence illumination with a Photometrics Coolsnap EZ cooled charge-coupled device (CCD) camera interfaced with ImageJ, and we quantified thresholded images using a function of particle analyzer in ImageJ (NIH). Percentage of cell death was calculated as EthD-1-positive cells divided by the total number of cells stained with 5 μg/mL Hoechst 33342 (Invitrogen, H1399) as a nuclear counterstain. Data are presented as fold change over the level of cell death in the sample treated with hydrogen peroxide alone.

Mice

2.5-, 3-, 5-, and 22-month-old C57BL/6 female and male mice were obtained from Charles River or the National Institute of Aging animal colony. All animal experiments were performed according to an approved Institutional Animal Care and Use Committee protocol at the University of Missouri-Kansas City (UMKC), conforming to relevant federal guidelines. The UMKC animal facility is operated as a specific pathogen-free, AAALAC-approved facility. Animal care and husbandry meet the requirements in the Guide for the Care and Use of Laboratory Animals by the National Research Council. Animals were group housed and maintained on a 12-hr light/dark cycle with *ad libitum* food and water at a constant temperature of 23°C. Daily health check inspections were performed by qualified veterinary staff and/or animal care technicians.

Hindlimb Unloading with or without L-BAIBA

Paired 5-month-old male mice from the same litter (total 6 pairs from 3 litters) or paired 3-month-old female mice from the same litter (total 6 pairs from 4 litters) were assigned to either control or treated and housed in one large cage (10 × 19 × 11 in., 190 in^2 floor space). We chose 3-month-old female mice since by 5 months of age most of the trabecular bone is gone, while sufficient for quantitation at 3 months. They show 15%–50% lower values in trabecular bone parameters compared to 5-month-old male mice. The animals were weight-matched (male/control, 34.11 ± 4.20 g; L-BAIBA, 34.35 ± 4.23 g; female/control, 21.54 ± 1.08 g; L-BAIBA, 21.37 ± 1.88 g). L-BAIBA (100 mg/kg/day, AdipoGen Life Sciences) was provided in drinking water *ad libitum*, and the amounts consumed were similar in both control (male, 7.76 ± 0.55 mL; female, 6.88 ± 0.08 mL) and treated mice (male, 8.13 ± 0.73 mL; female, 6.97 ± 0.06 mL). L-BAIBA intake was 106.75 ± 12.04 and 129.91 ± 6.24 mg/kg/day for male and female, respectively. Hindlimb unloading was carried out for 2 weeks as described previously (Ferreira et al., 2011), with some modifications (Maurel et al., 2016). Mice were suspended by a tail ring surgically inserted through inter-vertebral disc space. The tail ring was attached to the tail with a supportive steel wire by strips of adhesive tape for reinforcement. This system allows a 360-degree range of motion while maintaining approximately a 30-degree angle between the body axis and cage bottom to prevent the contact of hindlimbs to the floor.

After 2 weeks of hindlimb unloading, EDL and soleus were dissected for *ex vivo* muscle contractility analysis. The right tibia was dissected for *ex vivo* μCT and the left tibia for bone histomorphometry. Both femurs were used for real-time PCR after flushing bone marrow.

Live Imaging of Osteocyte Mitochondria

Confocal imaging of cultured osteocytes was conducted using a Leica TCS SP8 confocal microscope equipped with a 40×, 1.2W (water immersion) objective. Primary bone osteocytes from DMP1-GFP mice or MLO-Y4 cells were incubated with 200 nM MitoTracker Deep Red FM (Invitrogen, M22426) for 30 min at 37°C, for visualization of mitochondrial morphology and dynamics, or incubated with 50 nM TMRE (Invitrogen, T669) for 10 min at 37°C, for monitoring mitochondrial inner membrane potential as previously described (Wang et al., 2018; Yi et al., 2011; Zhou et al., 2010). MitoTracker Deep Red FM was excited at 633 nm and its emitted fluorescence was collected at 640–690 nm. TMRE was excited at 543 nm with the fluorescence collected at 560–620 nm. The live-cell imaging was conducted at room temperature. NIH ImageJ software was used for imaging processing and quantification of the fluorescence intensity of TMRE and MitoTracker Deep Red.

Statistical Analysis

Data were expressed as means ± SD. The statistical significance of the difference between mean values was determined by the following statistical methods, using Prism 7.0 (GraphPad) or IBM SSPS Statistics: muscle CM analysis, multifactorial ANOVA followed by simple effect test with least significant difference (LSD); μCT and bone histomorphometry analyses, one-tailed paired t test for analyzing *in vivo* and *ex vivo* μCT and bone histomorphometry data and paired t test or two-way ANOVA followed by sidak post hoc test for EF classification; muscle contraction analysis, data were statistically analyzed with one-tailed paired t test and two-way ANOVA followed by sidak post hoc test; quantification of cell death and ROS, one-way ANOVA followed by tukey post hoc test; real-time qPCR, one-tailed paired t test or multifactorial ANOVA followed by simple effect test with LSD. Differences were considered significant at $p < 0.05$.

Data and Accessibility

The original raw data this work have been deposited at Mendeley Data and are available at https://doi.org/10.17632/gydsk6dvm2.1

SUPPLEMENTAL INFORMATION

Supplemental Information includes Supplemental Experimental Procedures, five figures, and three movies and can be found with this article online at https://doi.org/10.1016/j.celrep.2018.01.041.

ACKNOWLEDGMENTS

We thank Mark Dallas for his help with the μCT measurements and Carrie Zhao for her assistance with maintenance of the mice. We thank Keith W. Condon

and Lilian I. Plotkin for their advice regarding bone histomorphometric analysis. This work was supported by NIH NIA P1PO1AG039355 (L.F.B.), the Histology Core of the Indiana Center for Musculoskeletal Health (ICMH) at IU School of Medicine, and the Bone and Body Composition Core of the Indiana Clinical Translational Sciences Institute (CTSI) from NIH NCATS CTSA UL1TR001108. J.Z. received support from NIH NIAMS R01 AR057404 and Bank of American Victor E. Speas Foundation.

AUTHOR CONTRIBUTIONS

Conceptualization, Y.K. and L.F.B.; Methodology, Y.K., W.G., J.Z., M.B., and L.F.B.; Investigation, Y.K., J.A.V., J.Y., H.V., and K.J.; Writing, Y.K. and L.F.B.; Funding Acquisition, L.F.B. and J.Z.; Resources, W.G., J.Z., and L.F.B.; Supervision, W.G., Y.K., M.B., and L.F.B.

DECLARATION OF INTERESTS

The authors declare no competing interests.

Received: July 21, 2017
Revised: November 3, 2017
Accepted: January 12, 2018
Published: February 6, 2018

REFERENCES

Almeida, M., and O'Brien, C.A. (2013). Basic biology of skeletal aging: role of stress response pathways. J. Gerontol. A Biol. Sci. Med. Sci. *68*, 1197–1208.

Bakewell, L., Burdge, G.C., and Calder, P.C. (2006). Polyunsaturated fatty acid concentrations in young men and women consuming their habitual diets. Br. J. Nutr. *96*, 93–99.

Basso, N., and Heersche, J.N. (2006). Effects of hind limb unloading and reloading on nitric oxide synthase expression and apoptosis of osteocytes and chondrocytes. Bone *39*, 807–814.

Begriche, K., Massart, J., Abbey-Toby, A., Igoudjil, A., Lettéron, P., and Fromenty, B. (2008). Beta-aminoisobutyric acid prevents diet-induced obesity in mice with partial leptin deficiency. Obesity (Silver Spring) *16*, 2053–2067.

Bellido, T., and Plotkin, L.I. (2011). Novel actions of bisphosphonates in bone: preservation of osteoblast and osteocyte viability. Bone *49*, 50–55.

Benefield, L.E., and Holtzclaw, B.J. (2014). Aging in place: merging desire with reality. Nurs. Clin. North Am. *49*, 123–131.

Blair, S.N., Kohl, H.W., 3rd, Barlow, C.E., Paffenbarger, R.S., Jr., Gibbons, L.W., and Macera, C.A. (1995). Changes in physical fitness and all-cause mortality. A prospective study of healthy and unhealthy men. JAMA *273*, 1093–1098.

Bonewald, L.F. (2011). The amazing osteocyte. J. Bone Miner. Res. *26*, 229–238.

Bonewald, L.F., Kiel, D.P., Clemens, T.L., Esser, K., Orwoll, E.S., O'Keefe, R.J., and Fielding, R.A. (2013). Forum on bone and skeletal muscle interactions: summary of the proceedings of an ASBMR workshop. J. Bone Miner. Res. *28*, 1857–1865.

Brotto, M., and Bonewald, L. (2015). Bone and muscle: Interactions beyond mechanical. Bone *80*, 109–114.

Cabahug-Zuckerman, P., Frikha-Benayed, D., Majeska, R.J., Tuthill, A., Yakar, S., Judex, S., and Schaffler, M.B. (2016). Osteocyte Apoptosis Caused by Hindlimb Unloading is Required to Trigger Osteocyte RANKL Production and Subsequent Resorption of Cortical and Trabecular Bone in Mice Femurs. J. Bone Miner. Res. *31*, 1356–1365.

Cavanaugh, D.J., Lee, H., Lo, L., Shields, S.D., Zylka, M.J., Basbaum, A.I., and Anderson, D.J. (2009). Distinct subsets of unmyelinated primary sensory fibers mediate behavioral responses to noxious thermal and mechanical stimuli. Proc. Natl. Acad. Sci. USA *106*, 9075–9080.

Colaianni, G., Cuscito, C., Mongelli, T., Pignataro, P., Buccoliero, C., Liu, P., Lu, P., Sartini, L., Di Comite, M., Mori, G., et al. (2015). The myokine irisin increases cortical bone mass. Proc. Natl. Acad. Sci. USA *112*, 12157–12162.

Dallas, S.L., Prideaux, M., and Bonewald, L.F. (2013). The osteocyte: an endocrine cell ... and more. Endocr. Rev. *34*, 658–690.

Dankbar, B., Fennen, M., Brunert, D., Hayer, S., Frank, S., Wehmeyer, C., Beckmann, D., Paruzel, P., Bertrand, J., Redlich, K., et al. (2015). Myostatin is a direct regulator of osteoclast differentiation and its inhibition reduces inflammatory joint destruction in mice. Nat. Med. *21*, 1085–1090.

Edwards, R.H., Hill, D.K., Jones, D.A., and Merton, P.A. (1977a). Fatigue of long duration in human skeletal muscle after exercise. J. Physiol. *272*, 769–778.

Edwards, R.H., Young, A., Hosking, G.P., and Jones, D.A. (1977b). Human skeletal muscle function: description of tests and normal values. Clin. Sci. Mol. Med. *52*, 283–290.

Ehrenborg, E., and Krook, A. (2009). Regulation of skeletal muscle physiology and metabolism by peroxisome proliferator-activated receptor delta. Pharmacol. Rev. *61*, 373–393.

Feng, J.Q., Huang, H., Lu, Y., Ye, L., Xie, Y., Tsutsui, T.W., Kunieda, T., Castranio, T., Scott, G., Bonewald, L.B., and Mishina, Y. (2003). The Dentin matrix protein 1 (Dmp1) is specifically expressed in mineralized, but not soft, tissues during development. J. Dent. Res. *82*, 776–780.

Ferreira, J.A., Crissey, J.M., and Brown, M. (2011). An alternant method to the traditional NASA hindlimb unloading model in mice. J. Vis. Exp. *49*, 2467.

Finkel, T. (2015). The metabolic regulation of aging. Nat. Med. *21*, 1416–1423.

Frikha-Benayed, D., Basta-Pljakic, J., Majeska, R.J., and Schaffler, M.B. (2016). Regional differences in oxidative metabolism and mitochondrial activity among cortical bone osteocytes. Bone *90*, 15–22.

Giltay, E.J., Gooren, L.J., Toorians, A.W., Katan, M.B., and Zock, P.L. (2004). Docosahexaenoic acid concentrations are higher in women than in men because of estrogenic effects. Am. J. Clin. Nutr. *80*, 1167–1174.

Hamrick, M.W., McNeil, P.L., and Patterson, S.L. (2010). Role of muscle-derived growth factors in bone formation. J. Musculoskelet. Neuronal Interact. *10*, 64–70.

Holzerová, E., and Prokisch, H. (2015). Mitochondria: Much ado about nothing? How dangerous is reactive oxygen species production? Int. J. Biochem. Cell Biol. *63*, 16–20.

Huang, J., Romero-Suarez, S., Lara, N., Mo, C., Kaja, S., Brotto, L., Dallas, S.L., Johnson, M.L., Jähn, K., Bonewald, L.F., and Brotto, M. (2017). Crosstalk between MLO-Y4 osteocytes and C2C12 muscle cells is mediated by the Wnt/β-catenin pathway. JBMR Plus *1*, 86–100.

Jähn, K., Lara-Castillo, N., Brotto, L., Mo, C.L., Johnson, M.L., Brotto, M., and Bonewald, L.F. (2012). Skeletal muscle secreted factors prevent glucocorticoid-induced osteocyte apoptosis through activation of β-catenin. Eur. Cell. Mater. *24*, 197–209, discussion 209–210.

Jilka, R.L., and O'Brien, C.A. (2016). The Role of Osteocytes in Age-Related Bone Loss. Curr. Osteoporos. Rep. *14*, 16–25.

Jilka, R.L., Noble, B., and Weinstein, R.S. (2013). Osteocyte apoptosis. Bone *54*, 264–271.

Joeng, K.S., Lee, Y.C., Lim, J., Chen, Y., Jiang, M.M., Munivez, E., Ambrose, C., and Lee, B.H. (2017). Osteocyte-specific WNT1 regulates osteoblast function during bone homeostasis. J. Clin. Invest. *127*, 2678–2688.

Jung, T.W., Hwang, H.J., Hong, H.C., Yoo, H.J., Baik, S.H., and Choi, K.M. (2015). BAIBA attenuates insulin resistance and inflammation induced by palmitate or a high fat diet via an AMPK-PPARδ-dependent pathway in mice. Diabetologia *58*, 2096–2105.

Karsenty, G., and Olson, E.N. (2016). Bone and Muscle Endocrine Functions: Unexpected Paradigms of Inter-organ Communication. Cell *164*, 1248–1256.

Kato, Y., Windle, J.J., Koop, B.A., Mundy, G.R., and Bonewald, L.F. (1997). Establishment of an osteocyte-like cell line, MLO-Y4. J. Bone Miner. Res. *12*, 2014–2023.

Kennedy, O.D., Herman, B.C., Laudier, D.M., Majeska, R.J., Sun, H.B., and Schaffler, M.B. (2012). Activation of resorption in fatigue-loaded bone involves both apoptosis and active pro-osteoclastogenic signaling by distinct osteocyte populations. Bone *50*, 1115–1122.

Kitase, Y., Barragan, L., Qing, H., Kondoh, S., Jiang, J.X., Johnson, M.L., and Bonewald, L.F. (2010). Mechanical induction of PGE2 in osteocytes blocks glucocorticoid-induced apoptosis through both the β-catenin and PKA pathways. J. Bone Miner. Res. *25*, 2657–2668.

Langlais, C., Hughes, M.A., Cain, K., and MacFarlane, M. (2015). In Vitro Assembly and Analysis of the Apoptosome Complex. Cold Spring Harb. Protoc. *2015*, pdb.prot087080.

Manolagas, S.C., and Parfitt, A.M. (2013). For whom the bell tolls: distress signals from long-lived osteocytes and the pathogenesis of metabolic bone diseases. Bone *54*, 272–278.

Maurel, D.B., Duan, P., Farr, J., Cheng, A.L., Johnson, M.L., and Bonewald, L.F. (2016). Beta-Catenin Haplo Insufficient Male Mice Do Not Lose Bone in Response to Hindlimb Unloading. PLoS ONE *11*, e0158381.

McNeil, B., and Dong, X. (2014). Mrgprs as Itch Receptors. In Itch: Mechanisms and Treatment, *Chapter 12*, E. Carstens and T. Akiyama, eds. (CRC Press/Taylor & Francis). https://www.ncbi.nlm.nih.gov/books/NBK200929/.

Mo, C., Romero-Suarez, S., Bonewald, L., Johnson, M., and Brotto, M. (2012). Prostaglandin E2: from clinical applications to its potential role in bone- muscle crosstalk and myogenic differentiation. Recent Pat. Biotechnol. *6*, 223–229.

Nakashima, T., Hayashi, M., Fukunaga, T., Kurata, K., Oh-Hora, M., Feng, J.Q., Bonewald, L.F., Kodama, T., Wutz, A., Wagner, E.F., et al. (2011). Evidence for osteocyte regulation of bone homeostasis through RANKL expression. Nat. Med. *17*, 1231–1234.

Nielsen, A.R., Mounier, R., Plomgaard, P., Mortensen, O.H., Penkowa, M., Speerschneider, T., Pilegaard, H., and Pedersen, B.K. (2007). Expression of interleukin-15 in human skeletal muscle effect of exercise and muscle fibre type composition. J. Physiol. *584*, 305–312.

Pedersen, B.K. (2011). Muscles and their myokines. J. Exp. Biol. *214*, 337–346.

Qin, Y., Peng, Y., Zhao, W., Pan, J., Ksiezak-Reding, H., Cardozo, C., Wu, Y., Divieti Pajevic, P., Bonewald, L.F., Bauman, W.A., and Qin, W. (2017). Myostatin inhibits osteoblastic differentiation by suppressing osteocyte-derived exosomal microRNA-218: A novel mechanism in muscle-bone communication. J. Biol. Chem. *292*, 11021–11033.

Rinholm, J.E., Vervaeke, K., Tadross, M.R., Tkachuk, A.N., Kopek, B.G., Brown, T.A., Bergersen, L.H., and Clayton, D.A. (2016). Movement and structure of mitochondria in oligodendrocytes and their myelin sheaths. Glia *64*, 810–825.

Roberts, L.D., Boström, P., O'Sullivan, J.F., Schinzel, R.T., Lewis, G.D., Dejam, A., Lee, Y.K., Palma, M.J., Calhoun, S., Georgiadi, A., et al. (2014). β-Aminoisobutyric acid induces browning of white fat and hepatic β-oxidation and is inversely correlated with cardiometabolic risk factors. Cell Metab. *19*, 96–108.

Shi, C.X., Zhao, M.X., Shu, X.D., Xiong, X.Q., Wang, J.J., Gao, X.Y., Chen, Q., Li, Y.H., Kang, Y.M., and Zhu, G.Q. (2016). β-aminoisobutyric acid attenuates hepatic endoplasmic reticulum stress and glucose/lipid metabolic disturbance in mice with type 2 diabetes. Sci. Rep. *6*, 21924.

Shinohara, T., Harada, M., Ogi, K., Maruyama, M., Fujii, R., Tanaka, H., Fukusumi, S., Komatsu, H., Hosoya, M., Noguchi, Y., et al. (2004). Identification of a G protein-coupled receptor specifically responsive to beta-alanine. J. Biol. Chem. *279*, 23559–23564.

Smith, H., and Dymond, B. (1963). The Determination of Beta-Amino-Isobutyric Acid in Urine. Clin. Chim. Acta *8*, 614–620.

Stern, A.R., Stern, M.M., Van Dyke, M.E., Jähn, K., Prideaux, M., and Bonewald, L.F. (2012). Isolation and culture of primary osteocytes from the long bones of skeletally mature and aged mice. Biotechniques *52*, 361–373.

Uno, M., Nishimura, S., Fukuchi, K., Kaneta, Y., Oda, Y., Komori, H., Takeda, S., Haga, T., Agatsuma, T., and Nara, F. (2012). Identification of physiologically active substances as novel ligands for MRGPRD. J. Biomed. Biotechnol. *2012*, 816159.

Urakawa, I., Yamazaki, Y., Shimada, T., Iijima, K., Hasegawa, H., Okawa, K., Fujita, T., Fukumoto, S., and Yamashita, T. (2006). Klotho converts canonical FGF receptor into a specific receptor for FGF23. Nature *444*, 770–774.

Valko, M., Leibfritz, D., Moncol, J., Cronin, M.T., Mazur, M., and Telser, J. (2007). Free radicals and antioxidants in normal physiological functions and human disease. Int. J. Biochem. Cell Biol. *39*, 44–84.

van Bezooijen, R.L., Roelen, B.A., Visser, A., van der Wee-Pals, L., de Wilt, E., Karperien, M., Hamersma, H., Papapoulos, S.E., ten Dijke, P., and Löwik, C.W. (2004). Sclerostin is an osteocyte-expressed negative regulator of bone formation, but not a classical BMP antagonist. J. Exp. Med. *199*, 805–814.

Vemula, H., Kitase, Y., Ayon, N.J., Bonewald, L., and Gutheil, W.G. (2017). Gaussian and linear deconvolution of LC-MS/MS chromatograms of the eight aminobutyric acid isomers. Anal. Biochem. *516*, 75–85.

Verborgt, O., Gibson, G.J., and Schaffler, M.B. (2000). Loss of osteocyte integrity in association with microdamage and bone remodeling after fatigue in vivo. J. Bone Miner. Res. *15*, 60–67.

Verborgt, O., Tatton, N.A., Majeska, R.J., and Schaffler, M.B. (2002). Spatial distribution of Bax and Bcl-2 in osteocytes after bone fatigue: complementary roles in bone remodeling regulation? J. Bone Miner. Res. *17*, 907–914.

Wang, H., Qian, J., Zhao, X., Xing, C., and Sun, B. (2017). β-Aminoisobutyric acid ameliorates the renal fibrosis in mouse obstructed kidneys via inhibition of renal fibroblast activation and fibrosis. J. Pharmacol. Sci. *133*, 203–213.

Wang, H., Yi, J., Li, X., Xiao, Y., Dhakal, K., and Zhou, J. (2018). ALS-associated mutation SOD1G93A leads to abnormal mitochondrial dynamics in osteocytes. Bone *106*, 126–138.

Xiong, J., Piemontese, M., Onal, M., Campbell, J., Goellner, J.J., Dusevich, V., Bonewald, L., Manolagas, S.C., and O'Brien, C.A. (2015). Osteocytes, not Osteoblasts or Lining Cells, are the Main Source of the RANKL Required for Osteoclast Formation in Remodeling Bone. PLoS ONE *10*, e0138189.

Yi, J., Ma, C., Li, Y., Weisleder, N., Ríos, E., Ma, J., and Zhou, J. (2011). Mitochondrial calcium uptake regulates rapid calcium transients in skeletal muscle during excitation-contraction (E-C) coupling. J. Biol. Chem. *286*, 32436–32443.

Zhou, J., Yi, J., Fu, R., Liu, E., Siddique, T., Ríos, E., and Deng, H.X. (2010). Hyperactive intracellular calcium signaling associated with localized mitochondrial defects in skeletal muscle of an animal model of amyotrophic lateral sclerosis. J. Biol. Chem. *285*, 705–712.

Zylka, M.J., Rice, F.L., and Anderson, D.J. (2005). Topographically distinct epidermal nociceptive circuits revealed by axonal tracers targeted to Mrgprd. Neuron *45*, 17–25.

Cell Reports, Volume *22*

Supplemental Information

β-aminoisobutyric Acid, L-BAIBA, Is a Muscle-Derived Osteocyte Survival Factor

Yukiko Kitase, Julian A. Vallejo, William Gutheil, Harika Vemula, Katharina Jähn, Jianxun Yi, Jingsong Zhou, Marco Brotto, and Lynda F. Bonewald

Supplemental Experimental Procedures

C2C12 Cells

C2C12 murine multipotent cells were cultured as previously described (Cai et al., 2009; Shen et al., 1997; Zhao et al., 2008) in DMEM/high glucose +10 % FBS (100 U/mL P/S) and were maintained at 40–70 % cell density in a 5% CO_2 incubator at 37°C.

Testing and characterization of C2C12 myotube conditioned media (MT-CM)

Preparation of MT-CM: C2C12 cells were plated at 6,500 cells/cm^2 in T75 flasks supplemented with 12 mL culture media/ flask. Cells were induced to form MTs by switching culture medium to DMEM + 2.5 % horse serum (100 U/mL P/S) at a cell density of 80–90 % (2-3 day post-seeding). Cells were then cultured for 5–6 day until multinucleated, spontaneously contracting MTs were formed. The CM was generated during a 24 h culture period by changing the culture medium to phenol red-free DMEM/high glucose + 0.1 % BSA (100 U/mL P/S). Prior to use, the produced CM was centrifuged at 500 g for 5 min at 4 °C to remove cells and cellular debris. A similar DNA to culture media volume ratio was achieved using the described methods to generate MT-CM.

Quantification of cell viability: The percentage of cell death was quantified using the trypan blue exclusion method following previously published procedures (Ahuja et al., 2003; Kitase et al., 2010). Briefly, cells were cultured overnight, washed with phosphate-buffered saline (PBS) and treated with or without MT-CM for 1 h at various concentrations using phenol red-free αMEM + 2.5 % FBS + 2.5 % CS (100 U/ mL P/S) as culture medium. After pre-treatment, cells were exposed to phenol red-free culture media with or without 1 μM dexamethasone (Sigma-Aldrich, D4902) for 6 h. Adherent cells were trypsinized and combined with non-adherent cells. Cells were incubated for 10 min with 0.1 % trypan blue (Sigma-Aldrich, T8154). A Neubauer hemocytometer was used to count viable, non-stained cells and dead or dying cells that demonstrate blue staining throughout the whole cell body. Experiments contained 4–6 biological replicates and on average 100 cells per replicate were counted. Also, cellular apoptosis via nuclear fragmentation was performed. Cells were fixed for 10 min at 4 °C in 2 % neutrally buffered paraformaldehyde and after treatment nuclei were stained with 0.25 mg/mL DAPI (Sigma-Aldrich, D9542) for 5 min. The percentage of apoptotic cells was determined counting cells with an impaired nuclear membrane that demonstrate nuclear blebbing *versus* non-impaired cells. Experiments contained 4–6 biological replicates and an average 100 cells per replicate were counted.

Size cutoff: Amicon® Ultra-4 Centrifugal Filter Units for i) 10kD (Merck, UFC801008) and ii) 3kD (Merck, UFC800308) were used according to manufacturer's instructions. MT-CM was separated at 2750 g, 4° C for 45 min -2h in a swing rotor centrifuge until $\geq$ 85% of the volume was filtrated. 10% of the filtrate and retentate were used for experiments (see above).

Trypsin digest: Trypsin digest was performed overnight at 37°C with 0.05% Trypsin (Sigma-Aldrich, T4799) added. The successful digest was verified by SDS-PAGE and digested MT-CM was used at 10% for viability experiments (see above).

UV: UV light exposure was done using the cell culture hood UV light. MT-CM was placed into a tissue culture plastic dish and exposed to UV light for 24 h at RT. Exposure to RT for 24 h without UV light does not affect the stability of MT factor (data not shown). UV-exposed MT-CM was used at 1% for viability experiments (see above).

Heat/Boiling: Exposure to heat was done in a water bath set to 100°C. MT-CM in a sealed container was brought to a boiling state for 15 min, cooled down to RT and used at 1% for viability experiments (see above).

Quantification of reactive oxygen species (ROS)

MLO-Y4 cells were plated at 1×10^4/cm^2 on a collagen-coated 96-well plate with 8 wells for each experimental condition. Representative examples of three independent experiments are shown. Cells were pretreated with varying concentrations of L-BAIBA in 0.5% FBS/ 0.5% CS/α-MEM for 1 h, followed by treatment with 0.3 mM hydrogen peroxide for 1 h in 0.5% FBS/ 0.5% CS/α-MEM to induce cell death. Cells were stained with 5 μM CellROX orange reagent (Molecular probe, C10443) for 30 min to detect cellular oxidative stress. CellROX orange fluorescence dye is non-fluorescent while in a reduced state but starts to exhibit bright orange fluorescence upon oxidation by ROS. Images were obtained using the Nikon fluorescence microscope and quantified signal intensity using ImageJ. Integrated Density obtained from thresholded images was normalized by cell number. The signal intensity was presented as fold change based on the value in control sample.

Micro-computed tomography

In vivo μCT images were taken to assess the changes of bone structure at two-time points, 2 days before hindlimb unloading as a baseline and 2 days before sacrifice as the endpoint. Mice were anesthetized with 75mg/kg ketamine/0.5mg/kg Dex-Dormitor and right tibia was scanned by X-ray μCT (vivaCT40; Scanco Medical AG) at 55 kV, 145 μA, high resolution, 19 mm voxel, 200 ms integration time. To confirm the results of *in vivo* μCT, *ex vivo* μCT was also conducted using the same right tibiae. The tibiae were dissected and fixed for 1 day in 4% paraformaldehyde, and then kept in 70% ethanol at 4C until use. Specimens were scanned at 55 kV, 145 μA, high resolution, 10.5 mm voxel, 200 ms integration time. Three-dimensional images reconstructed within the range of 1 mm from the most proximal metaphysis of tibiae were analyzed. Trabecular morphometry was studied by excluding the cortical bone from the endocortical borders using hand-drawn contours followed by thresholding (sigma=0.8, support=1, lower/upper threshold=245/1000=332 mg HA/cm^3, peel iteration=0), and was characterized by bone volume fraction (BV/TV), trabecular number (Tb.N), trabecular thickness (Tb.Th), trabecular spacing (Tb.Sp), and connectivity density (Conn.D). Changes in the trabecular parameters in *in vivo* μCT images were expressed as a percentage of the baseline.

Structure model index (SMI) has been frequently used as a method to determine the rod-or plate-like geometry of trabecular structures (Hildebrand and Ruegsegger, 1997) but Ellipsoid factor (EF) classification was introduced recently to replace the SMI (Salmon et al., 2015). EF classification was performed using *ex vivo* μCT binary images with the range of 0.1-0.6 mm from the most proximal metaphysis of tibiae and analyzed with ImageJ plugins, BoneJ (Doube et al., 2010) and 3D viewer (Schmid et al., 2010) to visualize three-dimensionally. EF images and histograms were obtained using the following sampling options. Sampling increment: 0.001mm, Vectors: 20, Skeleton points per ellipsoid: 1, Contact sensitivity: 10, Maximum interactions: 20 and Maximum drift: 0.02 that allows 90% of pixels classified by at least one ellipsoid. EF images contain EF values ranging from -1 (most oblate, black color) to +1 (most prolate, white color).

Bone Histomorphometry

Left tibiae were fixed with 4% paraformaldehyde at 4°C for 1 day and then demineralized in 10% EDTA/PBS pH7.4. The bones were subsequently washed with PBS and dehydrated in different ethanol baths for 4hr each. Bones were then paraffin embedded and paraffin sections (5 μm) were cut, dewaxed, rehydrated. To visualize osteoclasts sections were stained for TRAP using a modification of Erlebacher and Derynck (Erlebacher and Derynck, 1996). The modifications consisted of (1) substituting Fast Red TR 1,5-napthalenedisulfonate salt for the chromophore and (2) increasing the incubation period. The TRAP reaction was counterstained with toluidine blue in Sorenson's buffer (Stevens and Farncis, 1996) to reveal osteoid and osteoblasts. Bone histomorphometric parameters were evaluated using Osteomeasure software (OsteoMetrics, Inc.). The region of interest analyzed was 1 mm in length, 200μm below the growth plate, corresponding to the area analyzed by μCT on the contralateral tibia. Osteocyte apoptosis was detected by TdT-mediated dUTP nick-end labeling (TUNEL) using a modified version of a commercial kit (GeneCopoeia). The modifications comprised (1) exposing the sections after de-parafinization and rehydration to 10 mM citrate buffer (pH 6.0) for 5 minutes at 48° C and (2) permeabilization using 0.05% pepsin in 0.1N HCL for 4 minutes at 37°C. The TUNEL reaction was counterstained using 0.2% methyl green. TUNEL negative osteocytes were quantified to examine the osteocyte viability *in vivo.*

Ex vivo muscle contractility analysis

Mice were sacrificed by cervical dislocation after collecting blood samples and the EDL and soleus muscles were removed for contractility analysis as previously described (Thornton et al., 2011). Muscles were immediately placed into a dish containing a physiological buffer solution (144 mM NaCl; 5 mM KCl; 1 mM $MgCl_2$; 25 mM $NaHCO_3$; 2.5 mM $CaCl_2$; pH 7.40) with 10 mM glucose. This solution was continuously aerated with a 95/5% O_2/CO_2 mixture. EDL and soleus muscles were mounted vertically between two stimulating platinum electrodes and proximal and distal tendons were secured to adjustable isometric force transducers and to a fixed support, respectively. The muscles were immersed into 20 mL bathing chambers containing an oxygenated physiological buffer. PowerLab® Software (ADInstruments Inc.) was used to store and analyze force data. Stimulatory voltage was provided by an S88X dual pulse digital stimulator (Grass Products) (100 V, pulse duration, 1 ms; train duration, 500 ms). Muscles were lengthened until a single tetanus stimulation produced maximal force and remained at this optimal muscle length (L_0) for the duration of the experiment. The bathing solution was then increased to 37°C and maintained at this temperature by a heated water circulating pump. All data are presented as mean ± SD.

Equilibration: EDL and soleus muscles were next allowed a 30 min equilibration period during which time they were stimulated with intercalating high and low-frequency pulse trains spaced every 3 min which corresponded to maximal (T_{max}) and half maximal (½ T_{max}) isometric force, respectively (200/100Hz for EDL; 160/40Hz for soleus). The proposed stimulation protocol

aids with the study of the relative contributions of the contractile machinery (T_{max}) and the EC-coupling (½ T_{max}) to contractile function (Brotto et al., 2002; Thornton et al., 2011).

Force-Frequency Relationship: Following equilibration, the EDL and soleus muscles were stimulated to contract with frequencies ranging from 1-200 Hz with a periodicity of 3 min to generate the force vs. frequency (FF) relationship.

Force data: Muscle force is reported as absolute force (mN) and force normalized to the following muscle physiological cross-sectional area (PCSA, N/cm^2) equation as previously reported (de Paula Brotto et al., 2001; Park et al., 2012), with a small modification, in that, in our final length calculation we considered the length to ratio of muscle fibers for stretched muscles (tendon-to-tendon) of ex vivo muscles in contractility chambers. We used the previous factors reported for EDL (0.75) and SOL (0.85) by James et al (1995), which has also been consistently used by Talis and colleagues (Tallis et al., 2014; Tallis et al., 2017) . It essentially means that the actual muscle fiber size is smaller than the length of the measured stretched muscle. Since the PCSA is very sensitive to length, by adjusting to the length of the muscle fiber, force estimation is more precise. Thus, our final formula was:

Muscle force (N/cm^2) = (force (g) x (muscle length (cm) x 0.75 (EDL) or 0.85 (SOL) x 1.06 (muscle density))/ (muscle weight (g) x 0.00981).

Importantly, our normalized forces are well within the upper levels of forces reported by other groups when experiments are performed at 37ºC (Bonetto et al., 2015; James et al., 2013; Tallis et al., 2017; Wright et al., 2017).

Slope data: The slope of the rising edge of muscle contractions was measured 0-31 ms after the start of the peak.

Measurement of BAIBA in muscle conditioned media (CM)

Preparation of muscle CM: Muscle CM were prepared from intact EDL and soleus muscles dissected from 5- or 22-month-old C57BL/6 male (n=5 for each age group) and female (n=6 and 4 for each age group respectively) mice. Muscles were placed inside Radnotti Chambers containing 20 mL of Ringer's solution using a four-chamber system driven by an ADI-PowerLab Software. The experimental condition previously defined (Jahn et al., 2012) was used in this study with some modifications. Briefly, static CM was obtained by placing muscles in the chamber without stimulation for 30min. Next, the optimal length of muscle allowing it to achieve maximal force was determined by the length-force relationship followed by 30 min equilibration. The force *versus* frequency relationship was conducted by stimulating with frequencies ranging from 1–130 Hz. Muscles were then equilibrated with stimulatory trains of 500 ms, 90 Hz, repeated at every minute for 30 min to collect muscle CM 90 Hz.

Quantification of BAIBA in muscle CM: D- and L-BAIBA levels in muscle CM were quantified using our previously described multichannel LC-MS/MS approach (Vemula et al., 2017). Briefly, to 1 mL of muscle CM was added 3 µL of 10 µM D-alanine (Sigma-Aldrich, A7377) as an internal standard, and protein precipitated with 2 volumes of ice-cold acetone (Fisher Scientific). After 10 min on ice, the sample was centrifuged at 3000 g, and the supernatant was collected, freeze-dried, and redissolved in 50 µL of HPLC water (Alfa Aesar)/0.1% formic acid (Fisher Scientific). A 20 µL aliquot of this reconstituted sample was derivatized with 20 µL of 40 mM Marfey's reagent (Novabiochem) in acetone plus 5 µL of 1 M triethylamine (Fisher Scientific) in water. This Marfey's derivatization reaction was incubated at 37 ºC for 2.5 h, and the reaction quenched by adding 5 µL of 1 M HCl and 150 µL of HPLC water/25% acetonitrile (Alfa Aesar) /0.1% formic acid. Derivatized samples were then analyzed for D- and L-BAIBA levels by liquid chromatography-mass spectrometry (LC/MS) as described in detail previously (Vemula et al, 2017). In comparison with other isobaric (same mass) aminobutyric acid isomers which all have a parent ion (Q1) at 356.2 m/z in positive mode, Marfey's-BAIBA derivatives provide a characteristic fragment (Q3) at 192.2 m/z, which is unique to D- and L-BAIBA isomers.

Quantification of amino acids in muscle CM: Amino acid levels in EDL and SOL male muscle CM were determined using Marfey's derivatized samples by LC-MS/MS quantification as described previously (Bobba et al., 2012; Jamindar and Gutheil, 2010; Putty et al., 2011; Putty et al., 2013). The amino acid concentration was obtained by subtracting the values in Ringer buffer.

Real-time quantitative PCR (RT-qPCR)

Preparation of mouse long bones: Long bones were dissected from 2.5-, 5- and 22-month-old male (n=3, 5 and 3 for each age group respectively) and female (n=4, 5 and 5 for each age group respectively) mice. Osteocyte-enriched long bones and osteoblast fractions were obtained as described in the above. Femurs obtained from hindlimb-unloaded male mice were flushed

to remove bone marrow but not digested with a series of collagenase/EDTA to examine differential gene expressions as a whole bone. Bones were pulverized using Bessman Tissue Pulverizer chilled with liquid nitrogen.

Preparation of MLO-Y4 cells: MLO-Y4 cells were plated at $1\times10^4/cm^2$ on a collagen-coated 6-well plate (3-4 replicates per treatment). For examining receptor expression levels, the cells were harvested next day. For examining mitochondrial gene expression levels, the cells were pretreated with L-BAIBA in 0.5% FBS/ 0.5% CS/α-MEM for 1 h, followed by treatment with 0.3 mM hydrogen peroxide for 1 h in 0.5% FBS/ 0.5% CS/α-MEM to induce cell death.

Total RNA extractions were carried out using TRIzol Reagent (Ambion, 15596018) according to the manufacturer's instruction. 500 ng or 1 µg of purified RNA was reverse transcribed into cDNA at 37°C for 120 min using High Capacity cDNA Reverse Transcription Kit (Applied Biosystems, 4368813) in a final volume of 20 µl. 1 µl of 4 fold-diluted cDNA was used as a template for a final volume of 20 µl. Relative expression levels were obtained by the ΔΔCt method. The expression levels of Glycine receptors, *Glra1* (Primer Bank ID (Wang et al., 2012): 31982694a1), *Glra2* (33604080a1), *Glra3* (17978252a1), *Glra4* (21040223a1), *Glrb* (31981754a1), and *Mrgprd* (15546054a1) were examined by SYBR Green-based RT-qPCR. Expression levels of *Rn18s* (Mm04277571_s1, Applied Biosystems) were used as a reference for normalization. Real-time qPCR analysis of femurs obtained from hindlimb unloaded male mice for *Rankl* (Mm00441906_m1, Applied Biosystems), *Opg* (Mm01205928_m1, Applied Biosystems) and Sost (Mm00470479_m1, Applied Biosystems) was also performed. The expression levels of mitochondrial genes, *Cat* (6753272a1), *Sod1* (12805215a1), *Sod2* (31980762a1), *Gpx1* (6680075a1), *Gpx3* (15011841a1), *Gpx5* (6754062a1), *Gpx7* (13195626a1), *Cyc* (6681095a1), *Cox4i1* (6753498a1), *Cox4i2* (16716379a1), *Atp5b* (31980648a1), *Ppargc1a* (6679433a1), *Ppargc1b* (18875426a1), *Tfam* (1575501a1), *Nfr1* (31543343a1), *Foxo1* (34328255a1), *Foxo3* (9789951a1), *Tfeb* (6755736a1), *Nfe2l1* (31982173a1) were examined by SYBR Green-based RT-qPCR. Hydrolysis probes were also used for the detection of *Gpx4* (Mm.PT.58.28460496, IDT) and *Aaprα* (Mm00440939_m1, Applied Biosystems). *Gapdh* (Mm99999915_g1) was used as a reference for normalization.

<u>*Mrgprd* siRNA transfection</u>

Cationic lipid-mediated transfections using Lipofectamine 2000 (Invitrogen) were performed according to the manufacturers' protocols. MLO-Y4 cells were plated in a 6-well tissue culture plate at a density of 2- $4x10^3$ cells/cm^2. Next day, the media were replaced with antibiotic-free growth media. A complex of *Mrgprd* DsiRNA (mm.Ri.Mrgprd.13.1, 2, 3) or universal control DsiRNA (DS NC1) in a TriFECTa RNAi Kit (IDT) and Lipofectamine 2000 was added to the cells and slightly agitated to mix. After 48-72 h at 37 °C, the cells were used for Real-time qPCR analysis to verify *Mrgprd* mRNA expression or perform cell death assay.

<u>CRISPR/Cas9 genome editing</u>

MLO-Y4 cells were seeded at the density of $1x10^4$ cells/cm^2 in 2.5%FBS/2.5%CS/α-MEM with antibiotics on a 12- or 6-well plate coated with type I collagen. Next day, change media to 2.5%FBS/2.5%CS/α-MEM without phenol red and antibiotics. The Alt-R CRISPR-Cas9 System (IDT) was used for gene editing of *Mrgprd*. Selection of two suitable target sites for Cas9 protein/gRNA ribonucleoprotein complexes (Cas9 RNPs) were chosen by using web tools, CHOPCHOP and Cas-Designer (Park et al., 2015). The target sequences are MRGPRD1:5'-GATCCAGGTCACAAGGTCCA**TGG**-3', MRGPRD2:5'-TGAGCTGCAATGGCATGCAG**AGG**-3'. *Mrgprd* specific Alt-R CRISPR crRNA and tracrRNA oligos were duplexed to form sgRNA. The sgRNA was incubated with a Cas9 nuclease (RNA Bio, CP01) to assemble the ribonucleoprotein complex, which was delivered by cationic lipid-mediated transfection (Lipofectamine CRISPRMAX Cas9 Transfection Reagent, Invitrogen, 11668-019) and incubated for 3 days. After the treatment, cells were harvested for western blot analysis or detached by trypsin-EDTA and re-seeded in a 96-well plate for cell death assay.

<u>Western-blot Analysis</u>

After 72 h transfection, the cells were washed with cold PBS twice and lysed with RIPA buffer including a protease inhibitor (Sigma-Aldrich, P8340). The cell lysate and sample buffer were mixed and boiled for 5 minutes before loading on the gel. Proteins (10 µg) were separated by SDS-PAGE at 100 V and were transferred electrophoretically to a PVDF membrane at 60 V for 3 h. The membranes were blocked in a blocking solution overnight at 4°C and incubated with the primary antibody against MRGPRD (Abcam, ab155099) at 1: 2000 dilution overnight at 4°C. The blots were incubated with a peroxidase-linked anti-rabbit secondary antibody (Thermo Fisher Scientific, 32460) at 1: 5000 for 2 h at a room temperature. Afterward, the immunoblots were visualized with an enhanced chemiluminescence (ECL) detection kit (Thermo Fisher Scientific, 32132).

The analysis of band intensity was performed using a LAS-3000 Imager (Fujifilm) and ImageJ software (NIH). β-actin (A3854, Sigma-Aldrich) at 1: 25000 dilution was used for normalization of MRGPRD.

In the case of the Western-blot analysis for catalase and GPX4, MLO-Y4 cells were incubated with 5 μM L-BAIBA or 1 mM NAC for 24 h. After treatment, the cells were processed for western blot analysis with the primary antibodies, anti-catalase (Cell Signaling Technology, D5N7V), anti-GPX4 (Abcam, ab125066) at 1:2000 dilution and anti-GAPDH (Cell Signaling Technology, 5174S) at 1:10000 dilution followed by HRP-linked anti-mouse secondary antibody (Cell Signaling Technology, 7076S). Results were visualized with the ECL reagent. Densitometry evaluation was conducted using ImageJ software.

Videos

MLO-Y4 osteocyte cells were cultured in 35mm glass bottom dishes in α-MEM with 2.5% calf serum + 2.5% FBS. The cells were stained with 500nM MitoTracker Deep Red for 20 minutes at 37°C, then washed 7X with PBS. Using a Leica SP8 confocal microscope, xyt images were taken every 30 seconds, each video consists of 20 images.

Supplemental References

Ahuja, S.S., Zhao, S., Bellido, T., Plotkin, L.I., Jimenez, F., and Bonewald, L.F. (2003). CD40 ligand blocks apoptosis induced by tumor necrosis factor alpha, glucocorticoids, and etoposide in osteoblasts and the osteocyte-like cell line murine long bone osteocyte-Y4. Endocrinology *144*, 1761-1769.

Bobba, S., Resch, G.E., and Gutheil, W.G. (2012). A liquid chromatography-tandem mass spectrometry assay for detection and quantitation of the dipeptide Gly-Gln in rat brain. Analytical biochemistry *425*, 145-150.

Bonetto, A., Andersson, D.C., and Waning, D.L. (2015). Assessment of muscle mass and strength in mice. Bonekey Rep *4*, 732.

Brotto, M.A., Nosek, T.M., and Kolbeck, R.C. (2002). Influence of ageing on the fatigability of isolated mouse skeletal muscles from mature and aged mice. Experimental physiology *87*, 77-82.

Cai, C., Masumiya, H., Weisleder, N., Matsuda, N., Nishi, M., Hwang, M., Ko, J.K., Lin, P., Thornton, A., Zhao, X., et al. (2009). MG53 nucleates assembly of cell membrane repair machinery. Nat Cell Biol *11*, 56-64.

de Paula Brotto, M., van Leyen, S.A., Brotto, L.S., Jin, J.P., Nosek, C.M., and Nosek, T.M. (2001). Hypoxia/fatigue-induced degradation of troponin I and troponin C: new insights into physiologic muscle fatigue. Pflugers Arch *442*, 738-744.

Doube, M., Klosowski, M.M., Arganda-Carreras, I., Cordelieres, F.P., Dougherty, R.P., Jackson, J.S., Schmid, B., Hutchinson, J.R., and Shefelbine, S.J. (2010). BoneJ: Free and extensible bone image analysis in ImageJ. Bone *47*, 1076-1079.

Erlebacher, A., and Derynck, R. (1996). Increased expression of TGF-beta 2 in osteoblasts results in an osteoporosis-like phenotype. J Cell Biol *132*, 195-210.

Hildebrand, T., and Ruegsegger, P. (1997). Quantification of Bone Microarchitecture with the Structure Model Index. Computer methods in biomechanics and biomedical engineering *1*, 15-23.

Jahn, K., Lara-Castillo, N., Brotto, L., Mo, C.L., Johnson, M.L., Brotto, M., and Bonewald, L.F. (2012). Skeletal muscle secreted factors prevent glucocorticoid-induced osteocyte apoptosis through activation of beta-catenin. Eur. Cell Mater *24*, 197-209.

James, R.S., Staples, J.F., Brown, J.C., Tessier, S.N., and Storey, K.B. (2013). The effects of hibernation on the contractile and biochemical properties of skeletal muscles in the thirteen-lined ground squirrel, Ictidomys tridecemlineatus. J Exp Biol *216*, 2587-2594.

Jamindar, D., and Gutheil, W.G. (2010). A liquid chromatography-tandem mass spectrometry assay for Marfey's derivatives of L-Ala, D-Ala, and D-Ala-D-Ala: application to the in vivo confirmation of alanine racemase as the target of cycloserine in Escherichia coli. Analytical biochemistry *396*, 1-7.

Kitase, Y., Barragan, L., Jiang, J.X., Johnson, M.L., and Bonewald, L.F. (2010). Mechanical induction of PGE(2) in osteocytes blocks glucocorticoid induced apoptosis through both the beta-catenin and PKA pathways. J. Bone Miner. Res *25*, 2657-2668.

Park, J., Bae, S., and Kim, J.S. (2015). Cas-Designer: a web-based tool for choice of CRISPR-Cas9 target sites. Bioinformatics *31*, 4014-4016.

Park, K.H., Brotto, L., Lehoang, O., Brotto, M., Ma, J., and Zhao, X. (2012). Ex vivo assessment of contractility, fatigability and alternans in isolated skeletal muscles. Journal of visualized experiments : JoVE, e4198.

Putty, S., Rai, A., Jamindar, D., Pagano, P., Quinn, C.L., Mima, T., Schweizer, H.P., and Gutheil, W.G. (2011). Characterization of d-boroAla as a novel broad-spectrum antibacterial agent targeting d-Ala-d-Ala ligase. Chemical biology & drug design *78*, 757-763.

Putty, S., Vemula, H., Bobba, S., and Gutheil, W.G. (2013). A liquid chromatography-tandem mass spectrometry assay for d-Ala-d-Lac: a key intermediate for vancomycin resistance in vancomycin-resistant enterococci. Analytical biochemistry *442*, 166-171.

Salmon, P.L., Ohlsson, C., Shefelbine, S.J., and Doube, M. (2015). Structure Model Index Does Not Measure Rods and Plates in Trabecular Bone. Frontiers in endocrinology *6*, 162.

Schmid, B., Schindelin, J., Cardona, A., Longair, M., and Heisenberg, M. (2010). A high-level 3D visualization API for Java and ImageJ. BMC bioinformatics *11*, 274.

Shen, J., Bronson, R.T., Chen, D.F., Xia, W., Selkoe, D.J., and Tonegawa, S. (1997). Skeletal and CNS defects in Presenilin-1-deficient mice. Cell *89*, 629-639.

Stevens, A., and Farncis, R.J. (1996). Chapter 14: Micro-organisms. In Theory and Practice of Histological Techniques, 4th ed. J.C. Bancroft, and A. Stevens, eds. (New York: Churchill Livingstone), p. 766.

Tallis, J., Higgins, M.F., Cox, V.M., Duncan, M.J., and James, R.S. (2014). Does a physiological concentration of taurine increase acute muscle power output, time to fatigue, and recovery in isolated mouse soleus (slow) muscle with or without the presence of caffeine? Can J Physiol Pharmacol *92*, 42-49.

Tallis, J., Hill, C., James, R.S., Cox, V.M., and Seebacher, F. (2017). The effect of obesity on the contractile performance of isolated mouse soleus, EDL, and diaphragm muscles. J Appl Physiol (1985) *122*, 170-181.
Thornton, A.M., Zhao, X., Weisleder, N., Brotto, L.S., Bougoin, S., Nosek, T.M., Reid, M., Hardin, B., Pan, Z., Ma, J., et al. (2011). Store-operated Ca(2+) entry (SOCE) contributes to normal skeletal muscle contractility in young but not in aged skeletal muscle. Aging (Albany NY) *3*, 621-634.
Wang, X., Spandidos, A., Wang, H., and Seed, B. (2012). PrimerBank: a PCR primer database for quantitative gene expression analysis, 2012 update. Nucleic Acids Res *40*, D1144-1149.
Wright, L.E., Harhash, A.A., Kozlow, W.M., Waning, D.L., Regan, J.N., She, Y., John, S.K., Murthy, S., Niewolna, M., Marks, A.R., et al. (2017). Aromatase inhibitor-induced bone loss increases the progression of estrogen receptor-negative breast cancer in bone and exacerbates muscle weakness in vivo. Oncotarget *8*, 8406-8419.
Zhao, X., Weisleder, N., Thornton, A., Oppong, Y., Campbell, R., Ma, J., and Brotto, M. (2008). Compromised store-operated Ca2+ entry in aged skeletal muscle. Aging Cell *7*, 561-568.

Figure S1.

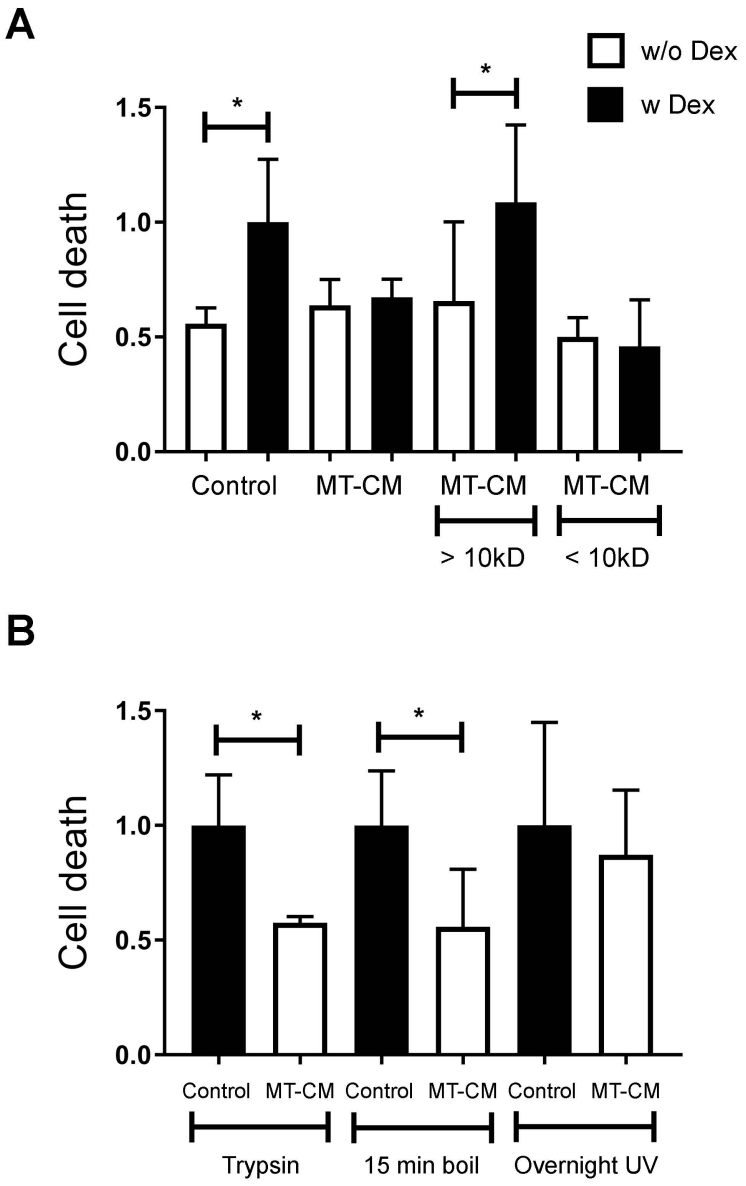

Figure S1. Low molecular weight muscle factors protect osteocytes from dexamethasone-induced cell death. Related to Figure 1.

(A) C2C12 myotube CM less than 10kD protects MLO-Y4 from cell death induced by dexamethasone. *$p<0.05$.
(B) The myotube CM retains the protective effect against cell death induced by dexamethasone after the treatment of trypsin and 15 min boiling, but not overnight UV exposure. *$p<0.05$.

Figure S2.

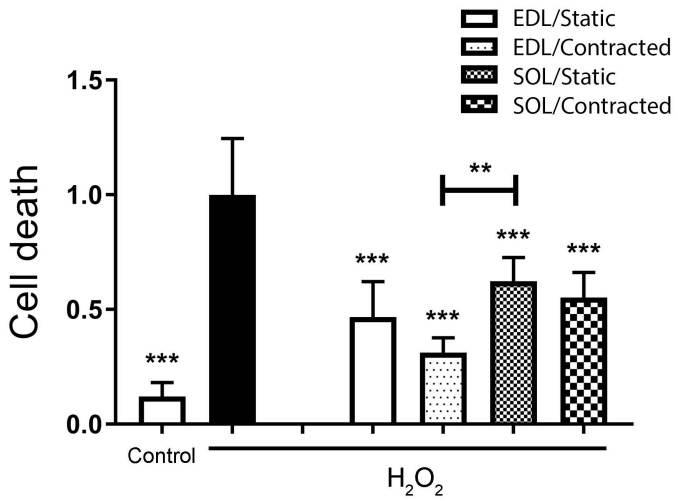

Figure S2. Both EDL and SOL secret factors that protect osteocytes from ROS-induced cell death. Related to Figure 1.

Both contracted and static EDL and SOL CMs obtained from 5-month-old male mice protect MLO-Y4 from cell death induced by H_2O_2. **p<0.01 and ***p<0.001 vs. H_2O_2.

Figure S3.

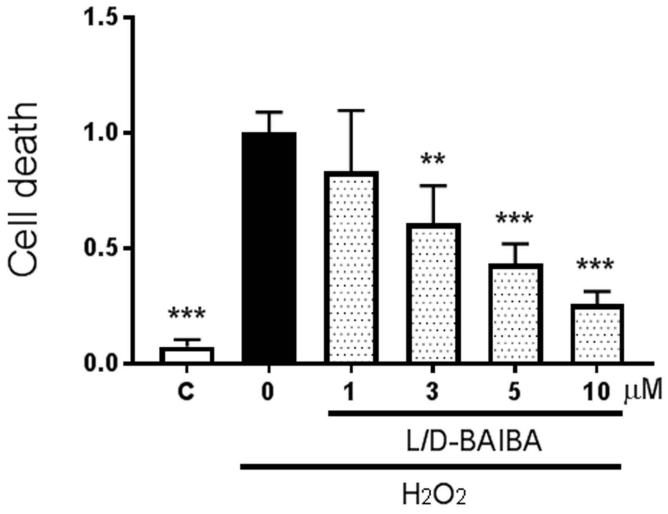

Figure S3. BAIBA protects osteoblasts from ROS-induced cell death. Related to Figure 1. BAIBA protects an osteoblast cell line, MC3T3-E1 from cell death induced by H_2O_2 in a dose-dependent manner. **p<0.01, ***p<0.001 vs. H_2O_2.

Figure S4.

A

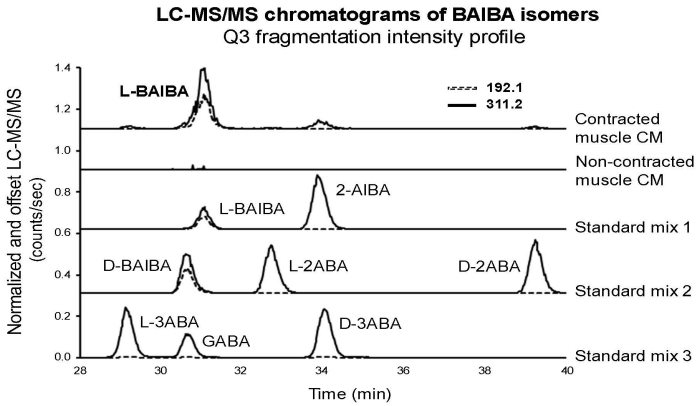

B

Amino acids in Msucle CM (μM)

Conc. (μM)	EDL 0Hz	SOL 0Hz	EDL 90Hz	SOL 90Hz
Gly	0.00	0.00	0.57	1.21
B-Ala	0.00	0.85	0.00	1.02
Ala	0.33	0.09	0.85	1.03
Arg	0.61	0.13	0.76	0.48
Asn	0.02	0.00	0.13	0.00
Asp	0.00	0.00	0.20	0.12
Gln	0.14	0.25	0.29	0.61
Glu	0.07	0.02	0.38	0.07
His	0.00	0.02	0.70	0.48
Iso	0.00	0.00	0.29	0.31
Lys	0.00	0.00	0.28	0.21
Met	0.05	0.04	0.02	0.06
Phe	0.06	0.05	0.25	0.28
Pro	0.00	0.00	0.32	0.39
Ser	0.00	0.00	0.79	0.92
Thr	0.00	0.00	0.39	0.52
Trp	0.00	0.02	0.07	0.07
Tyr	0.04	0.01	0.00	0.04
Val	0.00	0.00	0.51	0.61

** Leu was undetectable.

Figure S4. Muscle contraction increases the production of L-BAIBA, but not other isomers and amino acids. Related to Figure 5.

(A) Representative LC-MS/MS monitored chromatograms of BAIBA isomers in muscle conditioned media (top two chromatograms) and standard mixtures (bottom three chromatograms) illustrating selectivity of the Q3 = 92.1 fragment for BAIBA, and the ability to chromatographically resolve D- and L-BAIBA.

(B) Amino acids in muscle CM.

Figure S5.

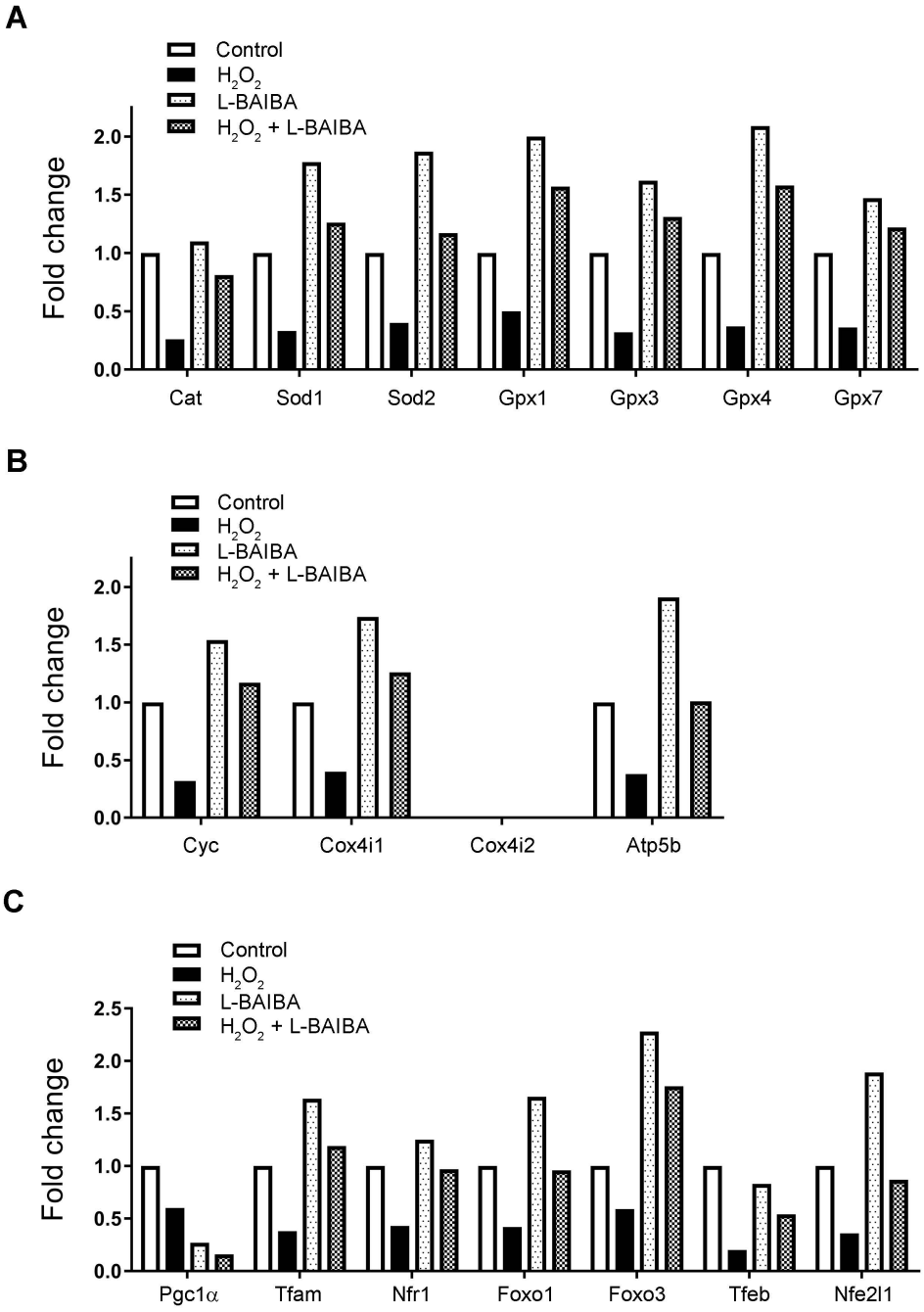

Figure S5. L-BAIBA regulates expression of mitochondrial genes. Related to Figure 7.
(A) RT-qPCR analysis of antioxidant enzyme gene expression in MLO-Y4 cells. Data are expressed as fold change over the expression level of each control. The average Ct values of the control are 27 for Cat, 23 for Sod1, 24 for Sod2, 24 for Gpx1, 27 for Gpx3, 29 for Gpx4, and 29 for Gpx7. Gpx5 is undetectable.
(B) RT-qPCR analysis of mitochondrial biogenesis-related gene expression in MLO-Y4 cells. Data are expressed as fold change over the expression level of each control. The average Ct values of the control are 21 for Cyc, 23 for Cox4i1, and 23 for Atp5b. Cox4i2 is undetectable.
(C) RT-qPCR analysis of transcriptional factor gene expression in MLO-Y4 cells. Data are expressed as fold change over the expression level of each control. The average Ct values of the control are 33 for Pgc1a, 27 for Tfam, 29 for Nfr1, 29 for Foxo1, 31 for Foxo3, 30 for Tfeb, and 26 for Nfe2l1. Pgc1b and Ppara are undetectable.